MODELING ELECTRICALLY SMALL APERTURES USING THE FINITE DIFFERENCE - TIME DOMAIN METHOD

by
NAYON TOMSIO

B.S. Electrical Engineering
University of Southern California
December 1992

Submitted to the Department of Electrical
Engineering and Computer Science in Partial
Fulfillment of the Requirements for the Degree of

MASTER OF SCIENCE

at the
MASSACHUSETTS INSTITUTE OF TECHNOLOGY
February 1997

Signature of Author_____

Department of Electrical Engineering and Computer Science
January 1997

Certified by_____

Professor Jin Au Kong
Thesis Supervisor

Certified by_____

Dr. Ying-Ching Eric Yang
Thesis Supervisor

Accepted by_____

Professor Arthur C. Smith
Chairman, Departmental Committee on Graduate Students

1

MODELING ELECTRICALLY SMALL APERTURES USING THE FINITE DIFFERENCE - TIME DOMAIN METHOD

by

NAYON TOMSIO

Submitted to the Department of Electrical Engineering and Computer Science
January 1997 in partial fulfillment of the requirements for the Degree of
Master of Science

ABSTRACT

A major cause of Electromagnetic Interference (EMI) from electrical equipment comes from inadequate shielding of the electronics. In the case of computers, the problem originates from apertures used to ventilate heat from the electronics of a computer to keep the computer cool and from apertures used for plugging input/output cables (e.g., mouse, keyboard, printer, video cables, etc.) into the computer chassis. It is such apertures that allow electromagnetic energy to escape the shielding enclosure, thereby causing EMI. The Finite Difference-Time Domain method is an excellent tool for analyzing scattering problems, provided there are enough spatial cells to provide good resolution of the small aperture. The challenge to this problem is to accurately describe the behavior of the aperture. The most direct way to solve this problem is to use the Brute Force method which requires the computational domain to be finely gridded. Despite being memory intensive and requiring rapidly increasing amounts of computational time to solve, it does provide somewhat accurate results. On the other hand, a more efficient method to accurately model the aperture is to use electric and magnetic dipoles to replace the aperture without increasing computer resources. This is called the Induced Dipole method.

The Induced Dipole method involves shorting the aperture so that only a solid metal plate remains. Then, a pair of oppositely directed magnetic and electric dipoles are placed on either side of where the aperture was located originally. This has been shown to work for small circular apertures. The intent is to apply this Induced Dipole method to circular apertures which are electrically small. For simplicity, the case of an infinite conducting plane with an electrically small aperture which is excited with an x-directed electric Hertzian dipole will be investigated in detail.

My main research objective is to model electrically small apertures accurately, without finely gridding the computational domain beyond 20 spatial cells per wavelength of highest frequency of interest. It is shown that the Induced Dipole method can model electrically small apertures as accurately as the Brute Force method with only a fraction of the computer resources. An analytical solution is derived to compare against the Induced Dipole method and the Brute Force method to determine their accuracy. This analytical solution is constructed using the analytical solution of Hertzian dipoles. The Induced Dipole method implemented with the Liao absorbing boundary condition, provides excellent

results compared to the analytical solution of the case of an infinite conducting plane with an electrically small circular aperture.

Thesis Supervisor: Professor Jin Au Kong

Title: Professor of Electrical Engineering

Thesis Supervisor: Dr. Ying-Ching Eric Yang

Title: Research Scientist, Research Laboratory of Electronics

ACKNOWLEDGEMENTS

5

To Joni

Contents

List of Figures

11

.

Chapter 1

Background

1.1   Electromagnetic Interference

Electromagnetic Interference (EMI) occurs when the electronics of one device affects the proper operation of another device or even with its own proper operation. A simple example of EMI is the nuisance caused when a hair dryer or a blender is being used which then creates unwanted static (snow) on the television. More serious concerns of EMI are the interference with critical equipment such as life support and monitoring equipment at hospitals, computer data centers, and airplanes' navigation equipment.

EMI from computers is rapidly becoming more difficult to control and even more difficult to predict. The reason is that computers are constantly being designed to run at higher frequencies causing harmonics of the clock to appear in the Microwave frequency band. The primary sources of EMI are the clock driver, the microprocessor, and the power supply. It is usually the clock driver of the computer that causes radiated EMI above 200 MHz because of its high spectral content due to the trapezoidal waveform [1] and the amount of power that is supplied to it to drive all the clock signals in the computer.

Secondary sources of EMI from computers are cables, resonances, and apertures. Small circular apertures like those used for ventilation of heat produced by the electronics of the computer system are of particular concern because they are a necessity and cannot be

covered up. These small circular apertures cause EMI problems especially at high frequencies; these problems are becoming exacerbated as computers are becoming faster (running at higher clock frequencies).

1.2   Related Research

The problem of determining the penetration of fields through apertures is by no means a new area of research [2]-[23]. In the early 1980's, the Finite Difference-Time Domain (FD-TD) method was being used to determine the penetration of an Electromagnetic Pulse (EMP), caused by nuclear detonation or lightning strike, through an aperture [2]-[4]. This work was more concerned with susceptibility and immunity of a computer from an aperture rather than how much EMI was generated from apertures of a computer; the analysis is the same but with different applications. The Thin-Slot Formalism [2]-[4] attempts to model a small aperture by increasing the permittivity seen by the electric field and proportionally decreasing the permeability as seen by the magnetic field. This method tends to average the electric field across the aperture, so as the aperture width decreases, the error increases since it underestimates the electric field. The Babinet principle can be used with the THREDE code [5] to solve the small aperture problem. THREDE is an older version of THREII code, used for the Thin-Slot Formalism, and is a scattered-field solver rather than a total field solver like THREII. The main problem with [5] is the results are not validated with other methods. There also have been codes which use a hybrid approach to solve this problem with the Method of Moments (MoM) and FD-TD method [6]. The small aperture problem can be solved using the Faraday's contour integral [7], but this method is intrinsically a two dimensional problem. An aperture also can be modeled in an infinite ground plane [8], but this limits the apertures to one infinite ground plane. Although I found plenty of research work done on modeling apertures using the FD-TD method, many did not address the problem of small apertures with subcell dimension widths [6], [8]-[11].

1.3   Description of Thesis

The purpose of my research is to accurately model electrically small apertures, where the diameter is smaller than a spatial cell (1/20 of a wavelength), using the Finite Difference-Time Domain method. An easy but computer intensive way of solving this problem is to increase the resolution of gridding so the FD-TD method could somewhat accurately calculate the fields that are scattered by the small aperture. The biggest problem with this Brute Force method is that it requires a tremendous amount of memory and time to solve the problem. I will attempt to model small apertures accurately without any need of reducing the size of the spatial cells by using electric and magnetic dipoles on either side of the small aperture. Oates [12] successfully modeled an electrically small round aperture, which was much smaller than a spatial cell, by modeling the small aperture using oppositely directed electric and magnetic dipoles on either side of the aperture, and short-circuiting the aperture. The central idea is to generate magnetic and electric current moments from the fields near the aperture. Once the current moments are accurately determined, the problem of finding the penetration of an incident field through a small aperture can be determined. Oates provided an accurate model of a small aperture by correctly specifying the current moments for a given size aperture. My work will expand on Oates work by increasing the accuracy of the Induced Dipole method by using a better absorbing boundary condition for the FD-TD method and using a more realistic excitation source.

Chapter 2

Finite Difference-Time Domain Method

2.1 Introduction

The Finite Difference-Time Domain method was first introduced by K. S. Yee in 1966 [24].
The method basically takes Maxwell's curl equations and transforms them into a set of
difference equations. Using the Yee grid, the H fields are located in the center of the cell
faces while the E fields are located on the center of the edges of the cell (see Figure 2.1).
The fields are updated every half time step, while using the leapfrog approach. The FD-TD
method did not become popular until the early 1980's for two reasons. First, the algorithm
requires that the computation domain be discretized to 20 cells per wavelength to obtain
accurate results. Unfortunately, this required an enormous amount of computer resources,
namely memory, which was not available at that time. It was not until the 1980's that there
were computers available to solve practical problems in a reasonable amount of time.
Another major problem with the FD-TD method was that spurious reflections were being
introduced by reflections at the borders of the computation domain. It was G. Mur that
developed the absorbing boundary conditions for the FD-TD method [25] that resolved the
problem of the spurious reflections.

The equations below are Maxwell's equations in differential form.

$$\nabla \times \overline{E} = -\frac{\partial \overline{B}}{\partial t} - \overline{J}_M \tag{2.1}$$

$$\nabla \times \overline{H} = \frac{\partial \overline{D}}{\partial t} + \overline{J}_E \tag{2.2}$$

$$\nabla \cdot \overline{B} = \rho_m \tag{2.3}$$

$$\nabla \cdot \overline{D} = \rho_e \tag{2.4}$$

In perfect conducting media and free space, (2.1) and (2.2) become (2.5) and (2.6), respectively.

$$\frac{\partial \overline{H}}{\partial t} = -\frac{1}{\mu_0}(\nabla \times \overline{E}) - \frac{1}{\mu_0}\overline{J}_M \tag{2.5}$$

$$\frac{\partial \overline{E}}{\partial t} = \frac{1}{\varepsilon_0}(\nabla \times \overline{H}) - \frac{1}{\varepsilon_0}\overline{J}_E \tag{2.6}$$
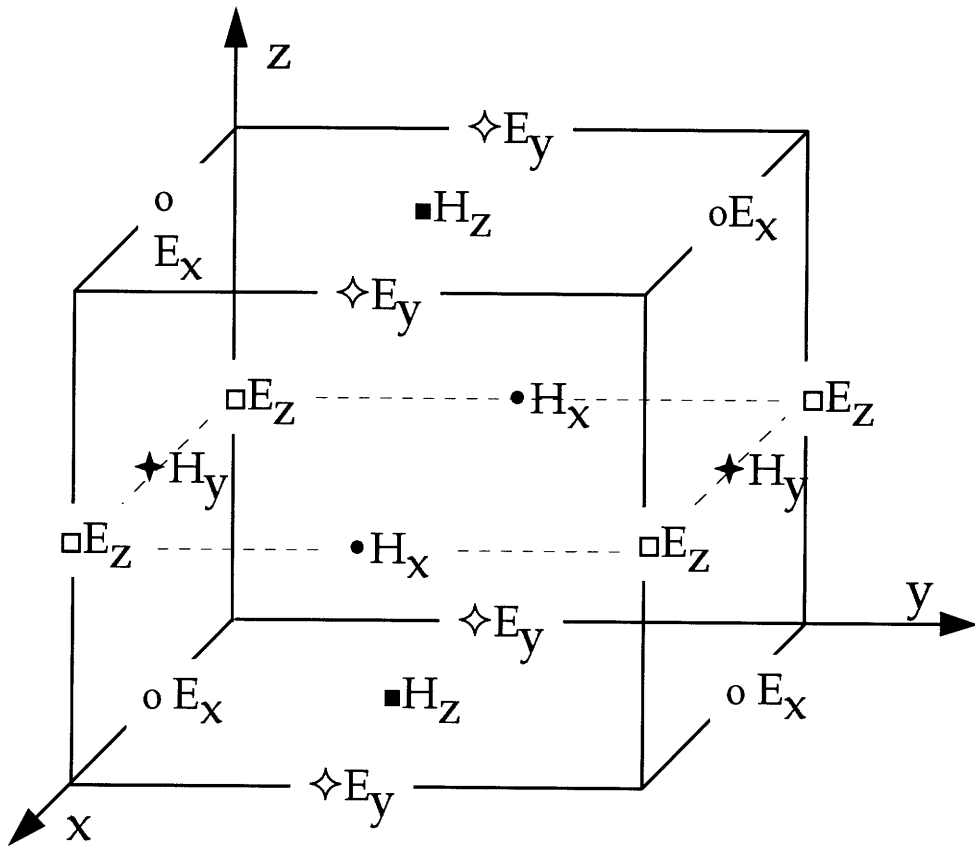
Figure 2.1: Yee Grid

2.2   FD-TD Discretized Equations

The Maxwell curl equations can then be discretized in both space and time. The computational domain of the FD-TD method represents the space of interest that the FD-TD method will solve Maxwell's equations. This space of interest is divided into cubes with dimensions Δx, Δy, and Δz. Each of these cubes utilizes the Yee grid convention. The following equations are the representation of discretized time (2.7) and space (2.8).

$$t = n\Delta t \tag{2.7}$$

$$(x, y, z) = (i\Delta x, j\Delta y, k\Delta z) \tag{2.8}$$

The corresponding difference equations for Maxwell's curl equations (2.5) and (2.6) are given in the equations (2.9)-(2.14) below.

$$\frac{E_x^n - E_x^{n-1}}{\Delta t} = \frac{1}{\varepsilon_0}\left(\frac{\Delta H_z^{n-\frac{1}{2}}}{\Delta y} - \frac{\Delta H_y^{n-\frac{1}{2}}}{\Delta z}\right) - \frac{1}{\varepsilon_0}J_{ex} \tag{2.9}$$

$$\frac{E_y^n - E_y^{n-1}}{\Delta t} = \frac{1}{\varepsilon_0}\left(\frac{\Delta H_x^{n-\frac{1}{2}}}{\Delta z} - \frac{\Delta H_z^{n-\frac{1}{2}}}{\Delta x}\right) - \frac{1}{\varepsilon_0}J_{ey} \tag{2.10}$$

$$\frac{E_z^n - E_z^{n-1}}{\Delta t} = \frac{1}{\varepsilon_0}\left(\frac{\Delta H_y^{n-\frac{1}{2}}}{\Delta x} - \frac{\Delta H_x^{n-\frac{1}{2}}}{\Delta y}\right) - \frac{1}{\varepsilon_0}J_{ez} \tag{2.11}$$

$$\frac{H_x^{n+\frac{1}{2}} - H_x^{n-\frac{1}{2}}}{\Delta t} = \frac{1}{\mu_0}\left(\frac{\Delta E_y^n}{\Delta z} - \frac{\Delta E_z^n}{\Delta y}\right) - \frac{1}{\mu_0}J_{mx} \tag{2.12}$$

$$\frac{H_y^{n+\frac{1}{2}} - H_y^{n-\frac{1}{2}}}{\Delta t} = \frac{1}{\mu_0}\left(\frac{\Delta E_z^n}{\Delta x} - \frac{\Delta E_x^n}{\Delta z}\right) - \frac{1}{\mu_0}J_{my} \tag{2.13}$$

$$\frac{H_z^{n+\frac{1}{2}} - H_z^{n-\frac{1}{2}}}{\Delta t} = \frac{1}{\mu_0}(\frac{\Delta E_x^n}{\Delta y} - \frac{\Delta E_y^n}{\Delta x}) - \frac{1}{\mu_0}J_{mz} \qquad (2.14)$$

The difference equations can then be represented using the Yee grid convention, where:

$$E_x^n(i,j,k) = E_x^{n-1}(i,j,k) + \frac{\Delta t}{\varepsilon_0}(\frac{H_z^{n-\frac{1}{2}}(i,j,k) - H_z^{n-\frac{1}{2}}(i,j-1,k)}{\Delta y})$$

$$-\frac{\Delta t}{\varepsilon_0}(\frac{H_y^{n-\frac{1}{2}}(i,j,k) - H_y^{n-\frac{1}{2}}(i,j,k-1)}{\Delta z}) - \frac{\Delta t}{\varepsilon_0}J_{ex} \qquad (2.15)$$

$$E_y^n(i,j,k) = E_y^{n-1}(i,j,k) + \frac{\Delta t}{\varepsilon_0}(\frac{H_x^{n-\frac{1}{2}}(i,j,k) - H_x^{n-\frac{1}{2}}(i,j,k-1)}{\Delta z})$$

$$-\frac{\Delta t}{\varepsilon_0}(\frac{H_z^{n-\frac{1}{2}}(i,j,k) - H_z^{n-\frac{1}{2}}(i-1,j,k)}{\Delta x}) - \frac{\Delta t}{\varepsilon_0}J_{ey} \qquad (2.16)$$

$$E_z^n(i,j,k) = E_z^{n-1}(i,j,k) + \frac{\Delta t}{\varepsilon_0}(\frac{H_y^{n-\frac{1}{2}}(i,j,k) - H_y^{n-\frac{1}{2}}(i-1,j,k)}{\Delta x})$$

$$-\frac{\Delta t}{\varepsilon_0}(\frac{H_x^{n-\frac{1}{2}}(i,j,k) - H_x^{n-\frac{1}{2}}(i,j-1,k)}{\Delta y}) - \frac{\Delta t}{\varepsilon_0}J_{ez} \qquad (2.17)$$

$$H_x^{n+\frac{1}{2}}(i,j,k) = H_x^{n-\frac{1}{2}}(i,j,k) - \frac{\Delta t}{\mu_0}(\frac{E_z^n(i,j+1,k) - E_z^n(i,j,k)}{\Delta y})$$

$$+\frac{\Delta t}{\mu_0}(\frac{E_y^n(i,j,k+1) - E_y^n(i,j,k)}{\Delta z}) - \frac{\Delta t}{\mu_0}J_{mx} \qquad (2.18)$$

$$H_y^{n+\frac{1}{2}}(i,j,k) = H_y^{n-\frac{1}{2}}(i,j,k) - \frac{\Delta t}{\mu_0}(\frac{E_x^n(i,j,k+1) - E_x^n(i,j,k)}{\Delta z})$$

$$+\frac{\Delta t}{\mu_0}(\frac{E_z^n(i+1,j,k)-E_z^n(i,j,k)}{\Delta x})-\frac{\Delta t}{\mu_0}J_{my} \qquad (2.19)$$

$$H_z^{n+\frac{1}{2}}(i,j,k)=H_z^{n-\frac{1}{2}}(i,j,k)-\frac{\Delta t}{\mu_0}(\frac{E_y^n(i+1,j,k)-E_y^n(i,j,k)}{\Delta x})$$

$$+\frac{\Delta t}{\mu_0}(\frac{E_x^n(i,j+1,k)-E_x^n(i,j,k)}{\Delta y})-\frac{\Delta t}{\mu_0}J_{mz} \qquad (2.20)$$

2.3   Accuracy and Stability of FD-TD Method

Accuracy of the FD-TD method is determined by the discretization of the computational domain. The finer the discretization (smaller Δx, Δy, Δz), the more accurate are the results from the FD-TD method. As a rule of thumb, accuracy is determined by the largest dimension of a discretization cell whose dimensions are Δx, Δy, Δz. This largest dimension must be 1/20 of a wavelength of the highest frequency of interest. The following equation is used to determine the highest frequency at which the results are still accurate:

$$f=\frac{c}{20\Delta_{max}} \qquad (2.21)$$

Stability of the FD-TD method is determined by the relationship of the dimensions of a discretization cell (Δx, Δy, Δz) to the time step Δt. The time step must satisfy the following equation, which is also know as the Courant stability condition [26]:

$$\Delta t\le\frac{1}{c}[\frac{1}{(\Delta x)^2}+\frac{1}{(\Delta y)^2}+\frac{1}{(\Delta z)^2}]^{-\frac{1}{2}} \qquad (2.22)$$

2.4   Absorbing Boundary Condition

Absorbing boundary conditions are an essential component to the Finite Difference-Time Domain method because they allow for the simulation of free space, a computational domain that is infinite, which has no artificial barriers. Without absorbing boundary conditions, the boundary of the computational domain would cause spurious reflections similar to those caused by perfectly conducting walls. This is ideal for those who want to simulate the behavior inside metal cavities and metal waveguides. Unfortunately, my research cannot take advantage of natural reflections caused by the boundary of the computational domain because I am mainly concerned with an infinite metal plate which can have a variety of apertures in free space.

This raises two important questions: 1) how to simulate an infinite metal plate; and, 2) what type of absorbing boundary to implement with the FD-TD method? Fortunately, both questions can be answered with one solution, which is to use the Liao absorbing boundary condition. The technique used to simulate an infinite metal plate is to run the metal plate into the boundaries of the computational domain. The problem occurs when one tries to use conventional Absorbing Boundary Conditions (ABC), such as Mur's first and second order ABC [25]. With Mur's second order boundary condition, there was a big problem with stability -- the FD-TD method blows up. The reason it blows up is because Mur's second order ABC requires fields that are tangential to the boundary. Thus, boundary conditions next to metal plates will attempt to pick up the E-fields (which are zero) of the perfectly conducting metal plate which eventually will cause the boundary condition to become unstable. Even if the metal plate does not run into a boundary but is within five grid spaces, the boundary condition remains unstable. If the metal plate does not run into a boundary, the ability to model an infinite metal plate is lost. Thus, it is impossible to model an infinite metal plate with Mur's second order ABC. However, it is possible to model an infinite metal plate with Mur's first order ABC, since it only requires the fields normal to the boundary. The problem is that any field that is not completely normal incidence to the boundary will cause Mur's first order ABC to reflect some of the field. The more the field

is off normal incidence, the more the field is reflected. Thus, Mur's first order ABC causes too many spurious reflection for accurate modeling of an infinite metal plate.

2.4.1   Liao Absorbing Boundary Condition

Another absorbing boundary condition is the Liao ABC [27]-[32]. The Liao ABC is an excellent choice for modeling infinite metal plates because it only requires normal fields to the boundary. The Liao ABC also has the added benefit of working under any order of accuracy, but experience shows that any order beyond second order becomes unstable. Actually, Liao's second order can become unstable, but can be easily fixed by introducing a tiny loss in $T_{1,1}$. The equations below are the Liao ABC for arbitrary order N. In equation (2.23), $u(t + \Delta t, x_1)$ represents the field that will be absorbed at boundary x_1. This equation is the generalized N-order Liao boundary condition.

$$u(t + \Delta t, x_1) \approx \sum_{j=1}^{N} (-1)^{j+1} C_j^N \overline{T}^j \overline{u}_j \qquad (2.23)$$

Also note that $\overline{T}^j$ represents row matrix and $\overline{u}_j$ represents a column matrix.

C_j^N is the binomial coefficient and is given below.

$$C_j^N = \frac{N!}{(N-j)! \, j!} \qquad (2.24)$$

As mentioned before $\overline{T}^j$ represents a row matrix of matrix $\overline{T}$, which is the interpolation matrix.

$$\overline{T}^j = [T_{j,1}, T_{j,2}, \cdots, T_{j,2j+1}] \qquad (2.25)$$

The first row matrix $\overline{T}^1$ is given below.

$$T_{1,1} = (2-s)(1-s)/2 \qquad (2.26)$$

$$T_{1,2} = s(2-s) \qquad (2.27)$$

$$T_{1,3} = s(s-1)/2 \qquad (2.28)$$

Where s is: $\qquad s = \dfrac{c\Delta t}{\Delta x} \qquad$ and $\qquad c = \sqrt{\mu\varepsilon}$

For $j \geq 2$, use the following recursion equation to find the $\overline{T}^{\,j}$ matrix rows.

$$\overline{T}^{\,j} = \overline{T}^{\,1}
\begin{bmatrix}
T_{j-1,1} & T_{j-1,2} & \cdots & \cdots & T_{j-1,2j-1} & 0 & 0 \\
0 & T_{j-1,1} & T_{j-1,2} & \cdots & \cdots & T_{j-1,2j-1} & 0 \\
0 & 0 & T_{j-1,1} & T_{j-1,2} & \cdots & \cdots & T_{j-1,2j-1}
\end{bmatrix} \qquad (2.29)$$

$\overline{u}_j^T$ is the transpose of field that is to be absorbed at the boundary.

$$\overline{u}_j^T = [u_{1,j}, u_{2,j}, \cdots, u_{2j+1,j}] \qquad (2.30)$$

where:

$$u_{i,j} = u(t_j, x_i) \qquad (2.31)$$

$$t_j = t - (j-1)\Delta t \qquad (2.32)$$

$$x_i = x_1 - (i-1)\Delta t \qquad (2.33)$$

There is a problem with Liao boundary conditions with N greater than 1. Basically, Liao second order (N=2) or greater boundary conditions become unstable. The Liao boundary condition can be stabilized [29] by introducing a minute amount of loss at the transmitting/absorbing boundary. This is easily achieved by modifying one element of the first row of the interpolation matrix ($\overline{T}^{\,1}$).

$$T_{1,1} = (2R_{loss} - s)(1-s)/2 \qquad (2.34)$$

where: $0.99 \leq R_{loss} \leq 1.00$ (2.35)

For my simulations, I used: $R_{loss} = 0.9925$ (2.36)

By adding this tiny amount of loss (R_{loss}), second order Liao boundary conditions become stabilized.

Thus far we have fully described a one-dimensional (along x) Liao boundary condition at the boundary x=1. The computational domain of the FD-TD method in three-dimensions has six boundaries, like a rectangular box. Thus, to obtain absorbing boundary conditions, the Liao boundary conditions must be applied to the tangential fields at each boundary. The Liao boundary conditions in three-dimensions are as follows:

For boundaries at: x=1 and x=nx: where u is applied to both tangential fields E_y and E_z

$$u(t + \Delta t, x_1) \approx \sum_{j=1}^{N} (-1)^{j+1} C_j^N \overline{T}_x^{\,j} \overline{u}_j \qquad (2.37)$$

$$u(t + \Delta t, x_{nx}) \approx \sum_{j=1}^{N} (-1)^{j+1} C_j^N \overline{T}_x^{\,j} \overline{u}_j \qquad (2.38)$$

For boundaries at: y=1 and y=ny: where u is applied to both tangential fields E_x and E_z

$$u(t + \Delta t, y_1) \approx \sum_{j=1}^{N} (-1)^{j+1} C_j^N \overline{T}_y^{\,j} \overline{u}_j \qquad (2.39)$$

$$u(t + \Delta t, y_{ny}) \approx \sum_{j=1}^{N} (-1)^{j+1} C_j^N \overline{T}_y^{\,j} \overline{u}_j \qquad (2.40)$$

For boundaries at: z=1 and z=nz: where u is applied to both tangential fields E_x and E_y

$$u(t + \Delta t, z_1) \approx \sum_{j=1}^{N} (-1)^{j+1} C_j^N \overline{T}_z^{\,j} \overline{u}_j \qquad (2.41)$$

$$u(t + \Delta t, z_{n_z}) \approx \sum_{j=1}^{N} (-1)^{j+1} C_j^N \overline{T}_z^j \overline{u}_j \qquad (2.42)$$

Note: for uniform FD-TD gridding,

$$\overline{T}^j = \overline{T}_x^j = \overline{T}_y^j = \overline{T}_z^j \qquad (2.43)$$

$$s = s_x = s_y = s_z \qquad (2.44)$$

where,

$$s_x = \frac{c\Delta t}{\Delta x} \qquad s_y = \frac{c\Delta t}{\Delta y} \qquad s_z = \frac{c\Delta t}{\Delta z} \qquad (2.45)$$

Figure 2.2 compares the second order Mur and the second order Liao boundary conditions to the analytical solution for the case of x-directed electric dipole radiating in free space with no scatterer using a computational domain of 24 Δ x 24 Δ x 100 Δ, where each Δ=0.01m. It is immediately obvious that the Mur boundary condition causes spurious reflections, whereas the Liao boundary does not contain these reflections.

No Scatterer

Liao 2nd order vs Mur 2nd order vs Analytic
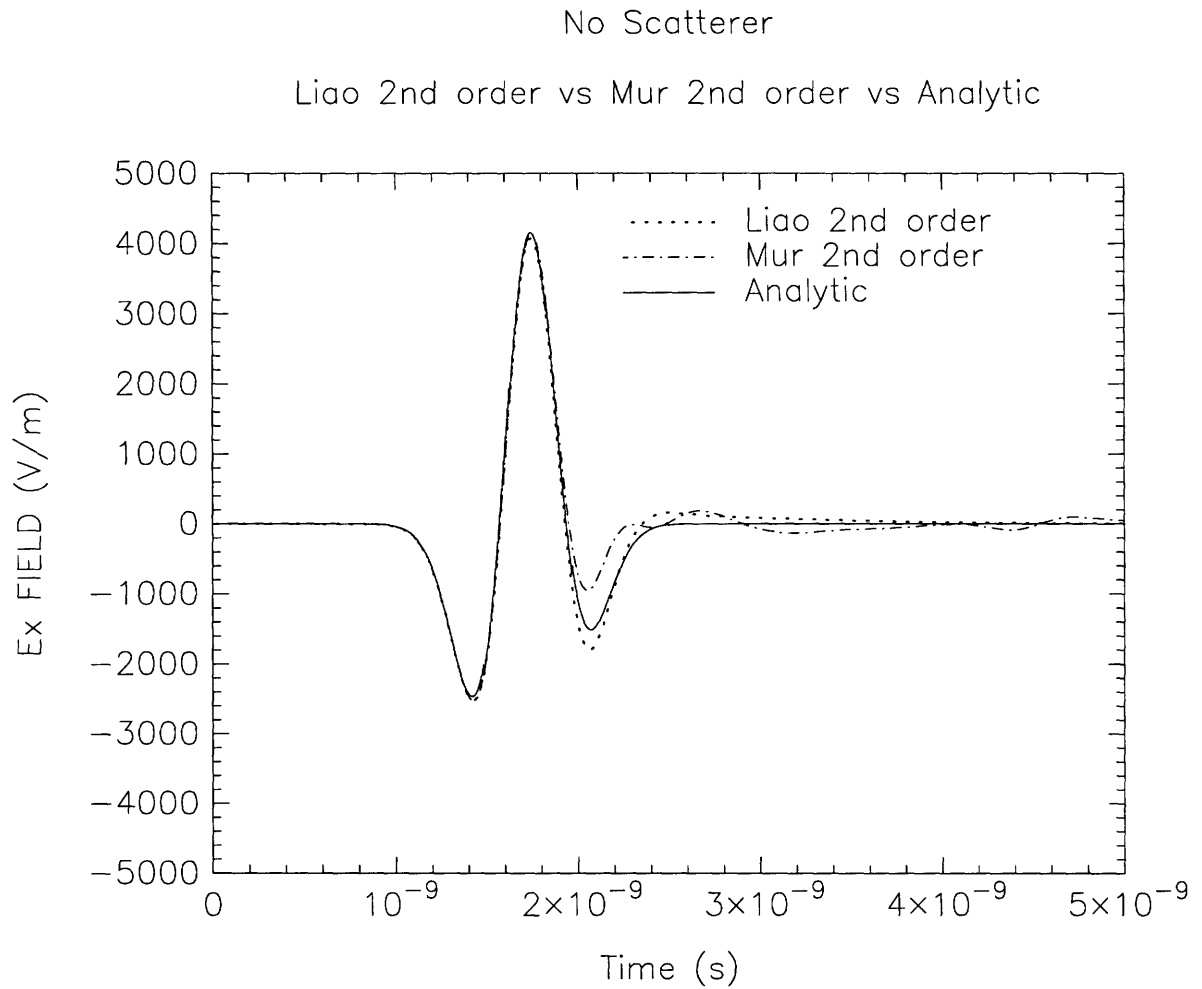
Figure 2.2: The analytical solution of the Ex field 0.2m away from an x-directed electric Hertzian dipole in free space compared to FD-TD method using Mur 2nd order and Liao 2nd order boundary conditions.

2.5   Sources

The Finite Difference-Time Domain (FD-TD) method requires an excitation source that must be specified so that fields propagate throughout the computational domain. The most common type of excitation sources are analytic plane waves, Hertzian magnetic dipoles, and Hertzian electric dipoles. Hertzian dipoles have infinitesimal dimensions. The Hertzian electric dipole is a current carrying element with infinitesimal length and a Hertzian magnetic dipole is a current loop with an infinitesimal radius. The type of source most applicable to what we want to model in reality, the computer enclosure with high-speed electronics inside, is Hertzian electric dipoles. The equation below, Equation 2.46, is the E-field produced by an x-directed Hertzian electric dipole for normal incident $\phi = 90°$ and for propagation along the negative z-axis $\theta = 180°$. In Chapter 4, Hertzian dipoles are derived.

$$\bar{E}(\bar{r}) = -i\omega\mu Il\frac{e^{ikr}}{4\pi r}\left\{\hat{\phi}\left[1+\frac{i}{kr}+\left(\frac{i}{kr}\right)^2\right]\right\} \tag{2.46}$$

Gaussian pulse in time: $I(t) = e^{-\alpha(t-\beta\Delta t)}$ (2.47)

where: $\alpha = (\frac{4}{\beta\Delta t})^2$ (2.48)

2β : pulse width   (2.49)

It is very common to use a current with Gaussian pulse waveform in the time domain to excite the Hertzian dipole because it is simple to implement and it provides a smooth roll-off in the frequency domain. The biggest drawback to using a current with a Gaussian waveform with the FD-TD method is that it creates a static dipole field which never decays to zero, which could later cause numerical problems. A better waveform to use for the current in the time domain is a doublet. A doublet is the time derivative of the Gaussian.

$$I(t) = -\alpha e^{-\alpha(t-\beta\Delta t)} \tag{2.50}$$

The doublet is also easy to implement and provides smooth roll-off in the frequency domain. Most importantly, it eliminates any static dipole field. One way to understand this phenomenon is to imagine the positive values of the doublet as creating the static dipole fields, while negative values of the doublet create an equal but opposite dipole fields which causes the static dipole fields to be eliminated. In Figure 2.3, we see the time domain doublet waveform of the dipole moment which is defined as the current multiplied by an infinitesimal length l. Figure 2.4 is frequency domain of the doublet.

Excitation Source: x—Directed Electric Dipole Moment
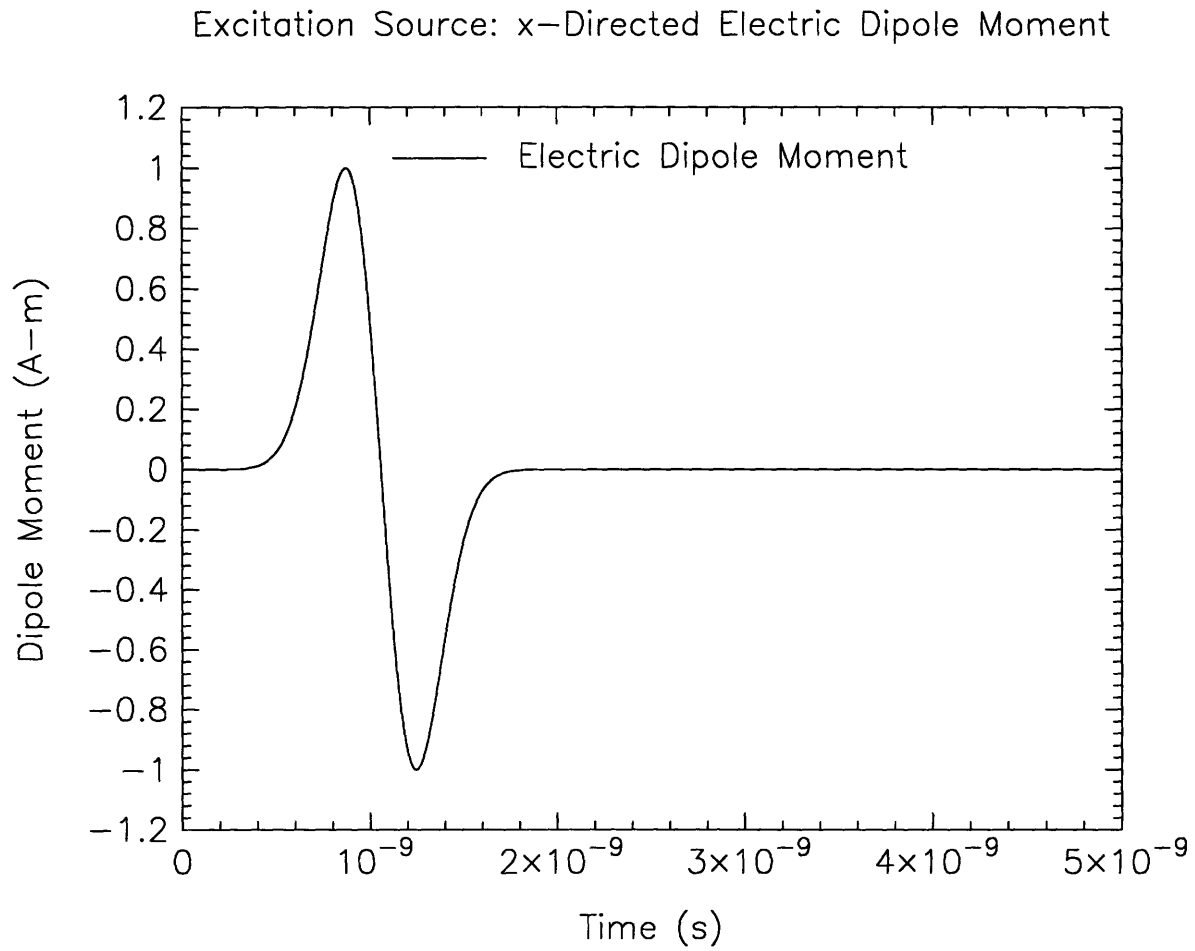
Figure 2.3: Time domain plot of an x-directed Hertzian electric dipole's dipole moment.
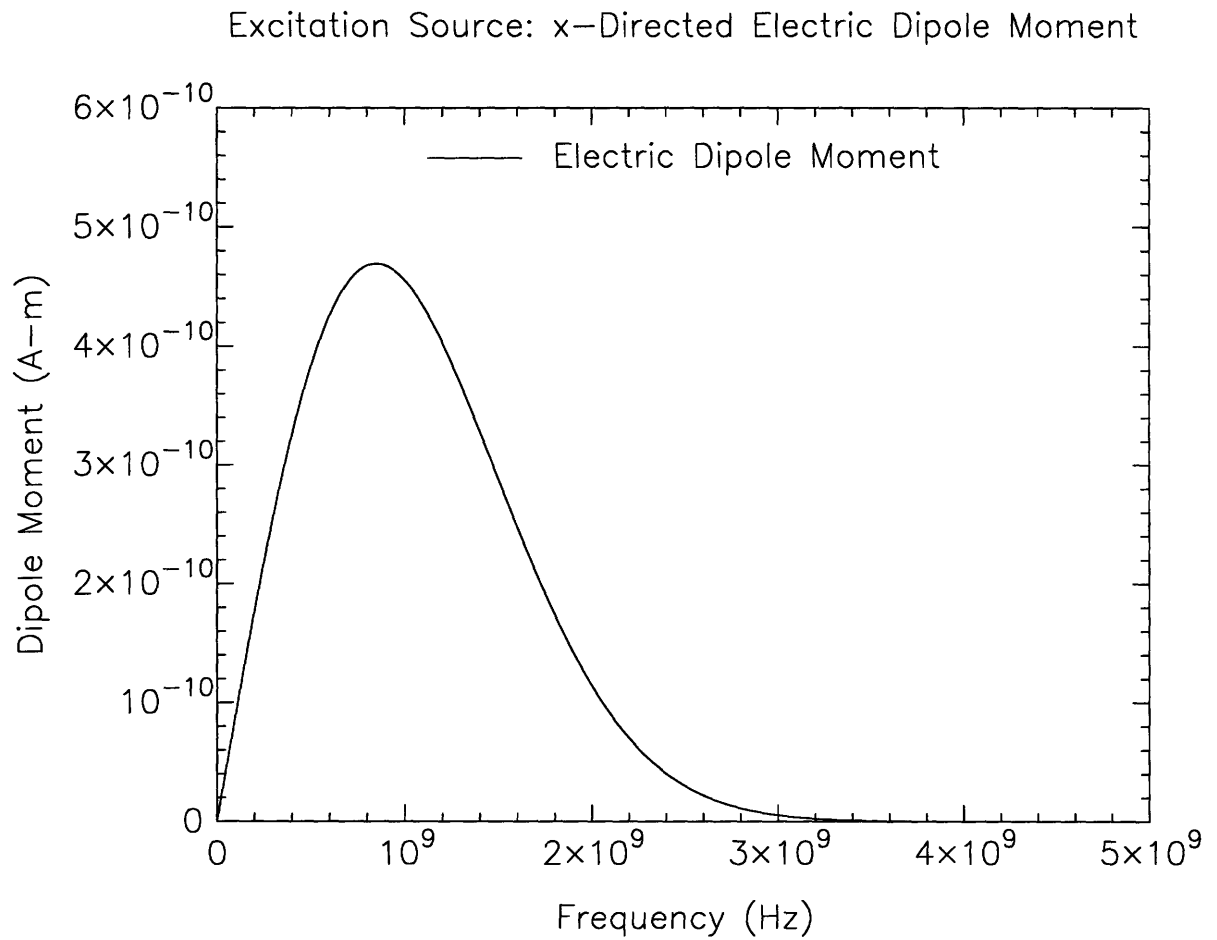
Figure 2.4: Frequency domain of an x-directed Hertzian electric dipole's dipole moment.

Chapter 3

Brute Force Method

3.1   Introduction

The Brute Force method uses the FD-TD method directly without any simplifying models or optimizations. In modeling electrically small apertures, the aperture is smaller than that of the gridding of the FD-TD method. Recall that the gridding of the FD-TD method is determined by the wavelength of the highest frequency of interest where gridding is such that there are 20 cells per wavelength. This gridding determines the accuracy of the FD-TD method up to the highest frequency.

3.2   Aperture Problem

One way to model this electrically small aperture is to make the gridding even finer than the 20 cells per wavelength so the aperture itself is represented by 80 cells as shown in Figure 3.1. Note that the FD-TD method using the Yee grid is confined to rectangular cubes or for uniform gridding, square cubes. These rectangular cubes have a problem representing non-orthogonal shapes (like circles, spheres, and triangles), which leads to a staircased approximation of the non-orthogonal shape. In the case of the circular aperture,
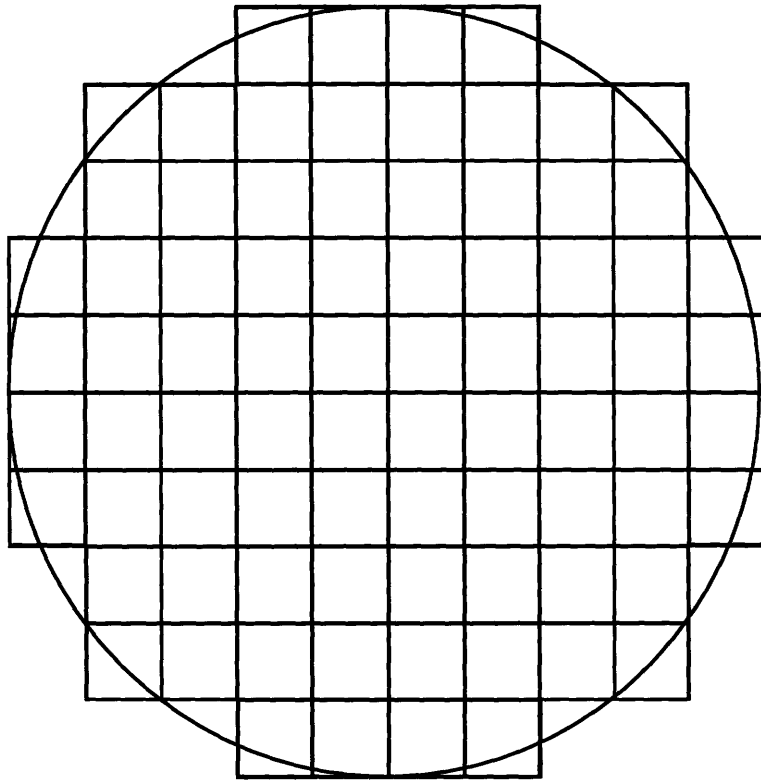
Figure 3.1: Brute Force gridding for aperture using 80 cells to represent the aperture.

we see that even with the 80 cells used to represent the aperture there is some staircasing involved.

The aperture problem that will be solved using three different methods is that of an infinite perfectly conducting plane (metal sheet) with an electrically small circular aperture as shown in Figure 3.2. This aperture problem will be excited using an x-directed Hertzian electric dipole as the source of electromagnetic energy. The infinite sheet is on z=0 plane, where the source is located on z>0 side of the plane and the observation points are on z<0 side of the plane. The distance from the excitation dipole source to aperture is r_{da} and the distance from the aperture to observation point is r_{ao} . The three methods that will be employed to solve this aperture problem are the: FD-TD Brute Force technique, analytical approach, and the Induced Dipole method.

The observation point is placed within the line of sight of the aperture and the excitation source, such that there is a line parallel to the z-axis connecting the excitation source, aperture, and the observation point. This simplification implies that only normally incident fields are considered as shown in the analytical solution to this aperture problem in Chapter 4. This is only a simplification and not a restriction to any of the three methods used to solve this aperture problem. For my simulations, the Brute Force method contains cubes of size: $\Delta x = \Delta y = \Delta z = 0.001m$ in dimension, computational domain of 120 x 120 x 500 cubes and

$$r_{da} = r_{ao} = 0.1m \qquad (3.1)$$

Figure 3.3 and Figure 3.4 show the results using the Brute Force method to solve the aperture problem described above for both the time and frequency domains, respectively. The FD-TD method provides results in the time domain; to obtain frequency domain results, a standard FFT was used. The results shown in Figures 3.3 and 3.4 must be verified using a different method. In Chapter 4, these results are compared to an approximate analytical solution to the aperture problem shown in Figure 3.2 for verification.
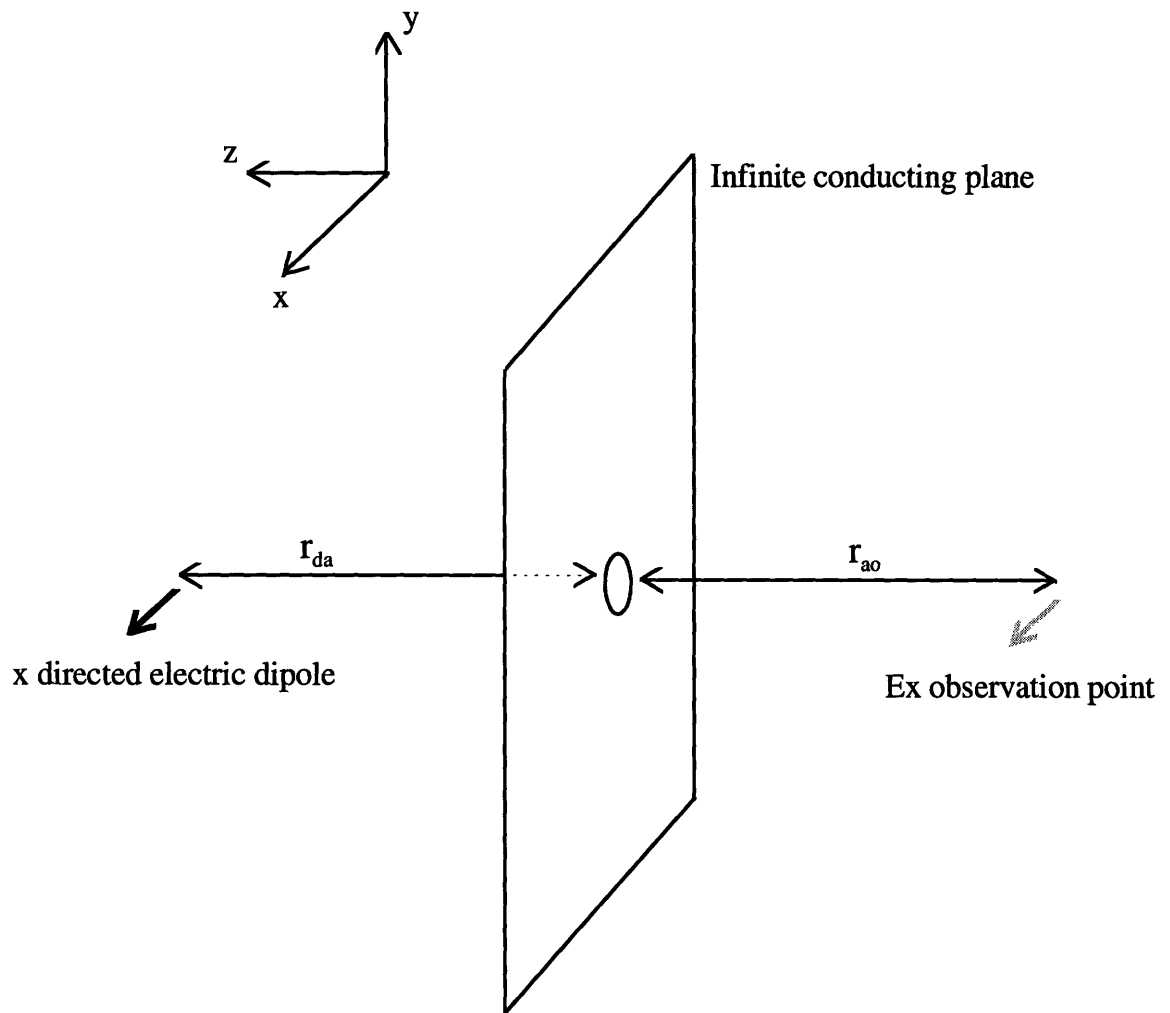
Figure 3.2: Representation of problem to be simulated, infinite conducting plane with an electrically small aperture.

Brute Force Method

Ex Field .1m from Aperture
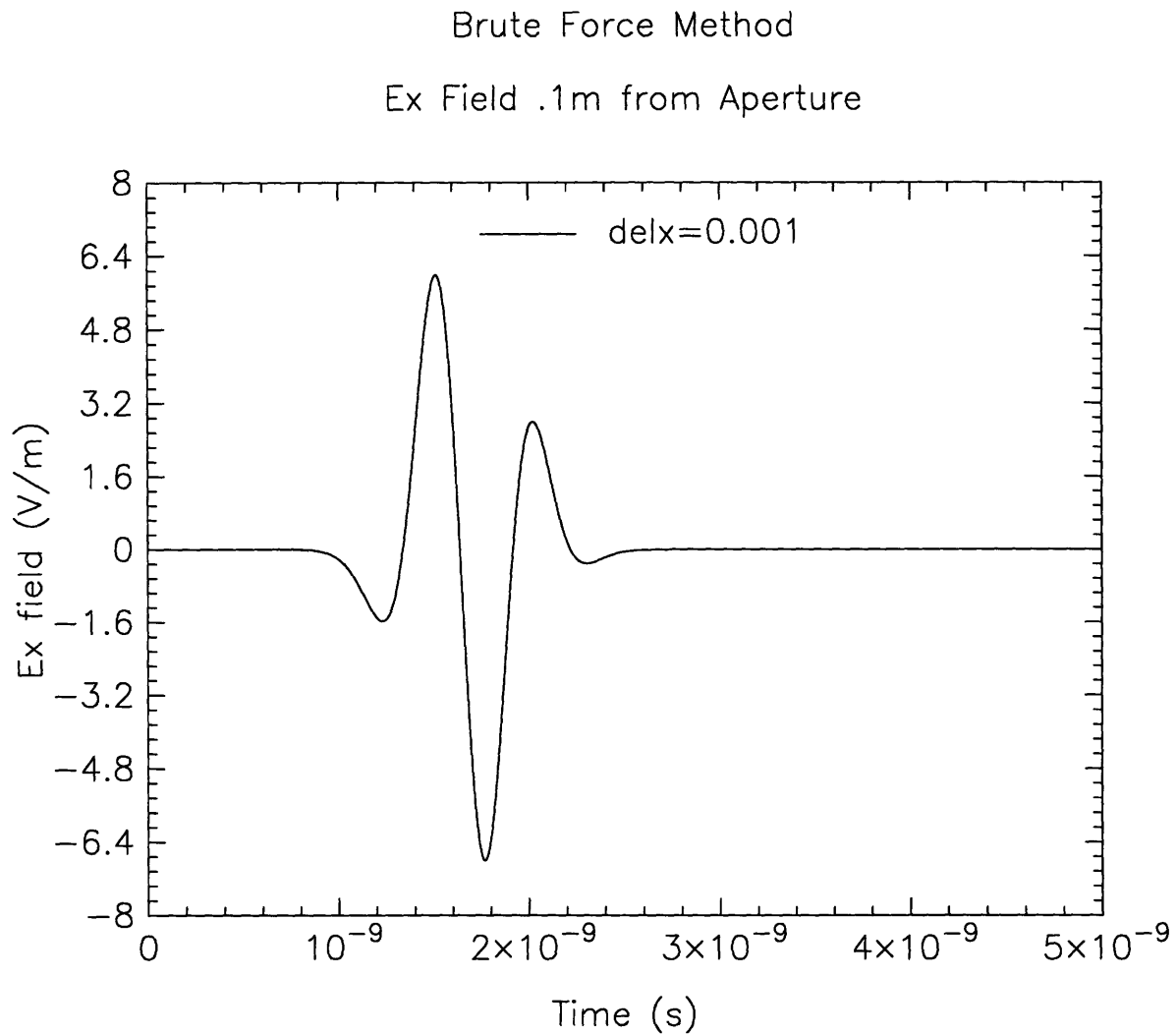
Figure 3.3: FD-TD simulation of an infinite ground plane with an aperture of radius 0.005m using the Brute Force method. The excitation source is 0.1m away from the aperture and the observation point is also 0.1m away.

Brute Force Method

Ex Field .1m from Aperture
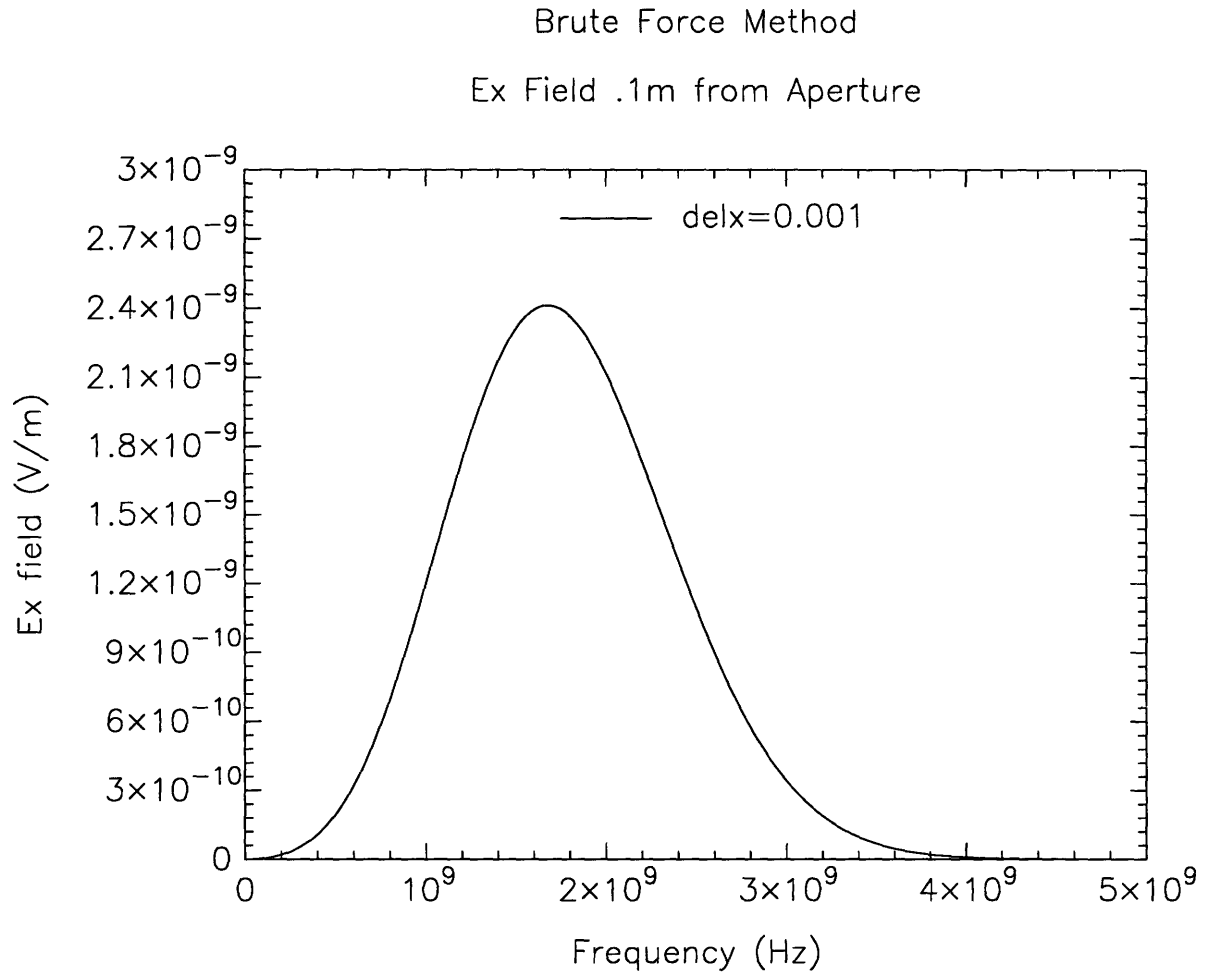
Figure 3.4: Frequency domain of FT-TD simulation of an infinite ground plane with an aperture of radius 0.005m using the Brute Force method. The excitation source is 0.1m away from the aperture and the observation point is also 0.1m away.

3.3   Hertzian Dipoles

Hertzian dipoles are an essential component to solving the aperture problem (described in Section 3.2) using the three methods (Brute Force, Analytical, and Induced Dipole). The Brute Force method uses an x-directed electric Hertzian dipole as an excitation source. For both the Analytical and Induced Dipole methods, an x-directed electric Hertzian dipole is used as an excitation source, in addition a y-directed magnetic Hertzian dipole is used to represent the aperture when excitation source, aperture, and observation point are in line of sight as shown in Figure 3.2.

Since these Hertzian dipoles are crucial to solving the aperture problem it is very important to verify that the Hertzian dipoles described above provide accurate results in the FD-TD method. The x-directed electric Hertzian dipole, as shown in Figure 3.5, is simulated using the FD-TD method by defining a electric dipole moment Il, as shown in Figure 2.3. To represent a dipole in FD-TD, the dipole moment Il must be converted to a current density (J_{ex}) to be used in the FD-TD equation (2.15). Similarly, a y-directed magnetic Hertzian dipole, as shown in Figure 3.6, is simulated using a magnetic dipole moment Kl which must be converted to current density (J_{my}) to be used in the FD-TD equation (2.19). I is the electric current; K is the magnetic current; and, l is the dipole length. In FD-TD, l is the grid dimension associated with direction of the dipole, for uniform gridding $\Delta=\Delta x=\Delta y=\Delta z$. The following equations convert dipole moments to current densities:

$$J_{ex} = \frac{Il}{\Delta^3} \tag{3.2}$$

$$J_{my} = \frac{Kl}{\Delta^3} \tag{3.3}$$
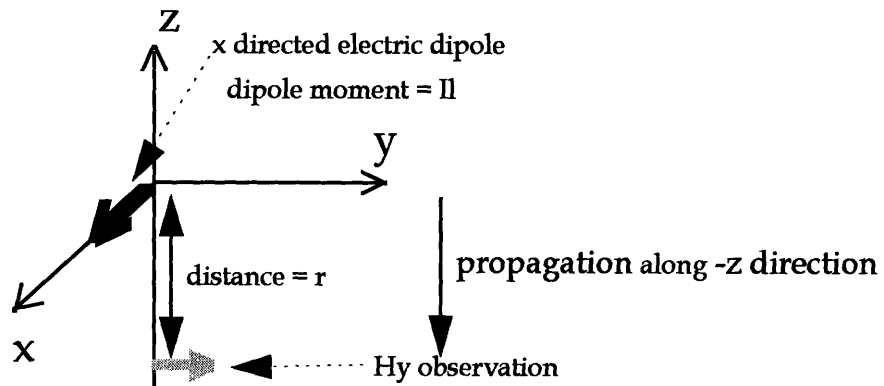
Figure 3.5: x-directed electric dipole with $\phi = 90°$ and $\theta = 180°$, so Hy is observable.
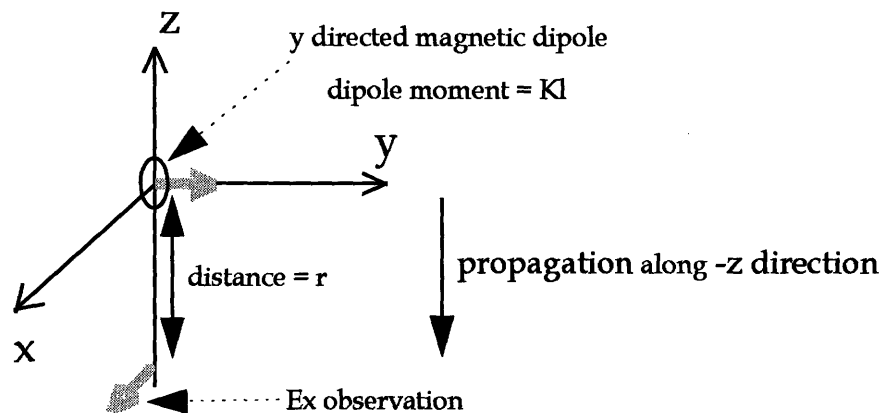
Figure 3.6: y-directed magnetic dipole with $\phi = 0°$ and $\theta = 180°$, so Ex is observable.

The FD-TD results of the Hertzian dipoles were obtained by using a computational domain gridded by 120 x 120 x 500 cells, where each grid cell dimension was $\Delta x = 0.001$m, $\Delta y = 0.001$m, $\Delta z = 0.001$m. Thus, the physical dimension of the uniformly gridded computation domain is 0.12m along the x, 0.12m along the y, and 0.5m along the z directions. Liao's 2nd order absorbing boundary conditions were used at the boundaries of the computation domain to simulate free-space propagation with no reflections.

For both the electric and magnetic dipole, the fields at observation point are normally incident and are propagating along the negative z-axis as defined by angles (ϕ, θ) as shown in Figures 3.5 and 3.6. The distance between the dipole and observation point (r) is 0.1m. Figure 3.7 and Figure 3.8 show the FD-TD result for an x-directed electric dipole and y-directed magnetic dipole, respectively. These results will also be verified by comparing them to the analytical solutions for x-directed electric dipole and y-directed magnetic dipole in Chapter 4.

Electric Hertzian Dipole x—directed

Hy Field .1m from Dipole
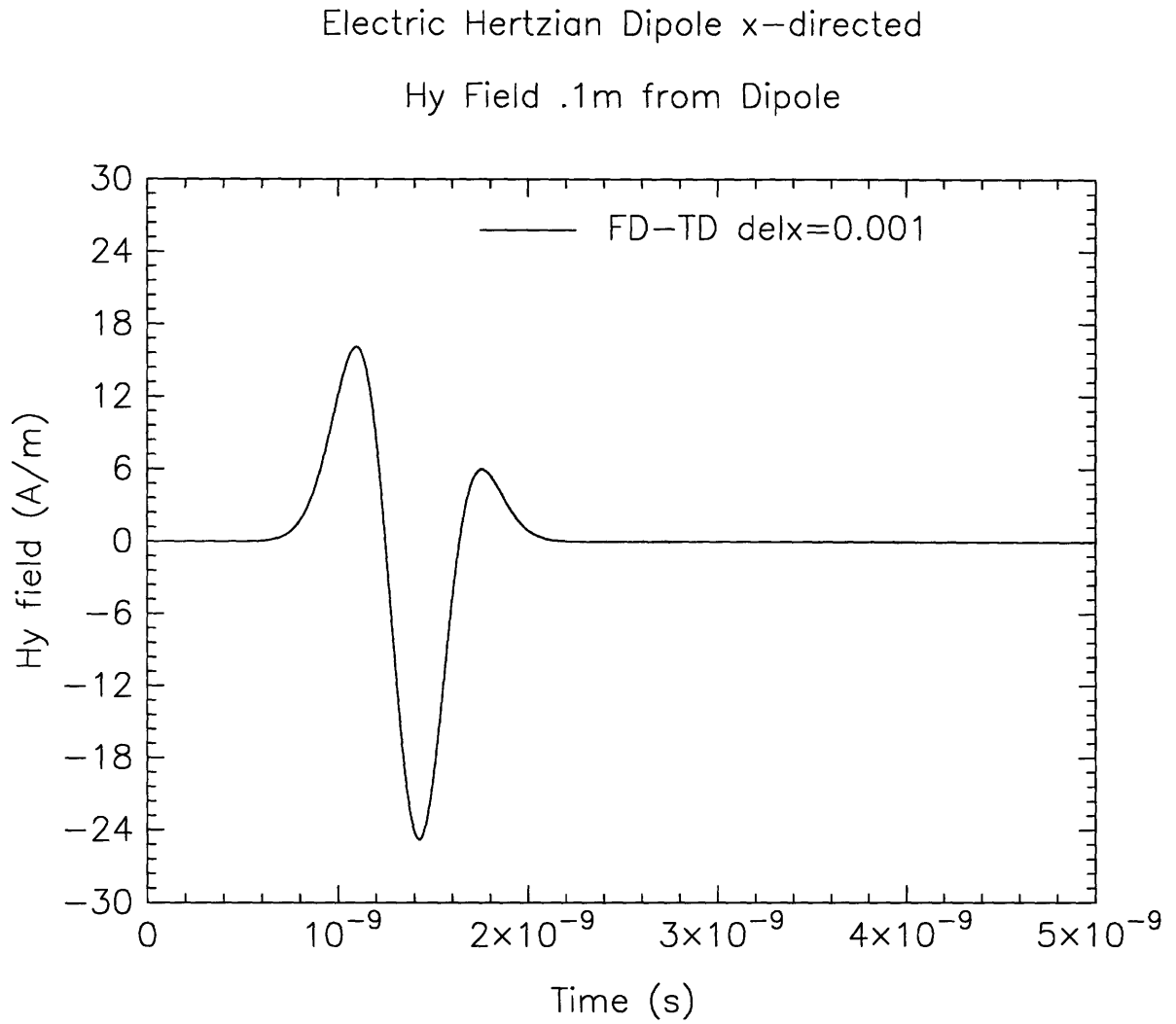
Figure 3.7: The Hy fields observed 0.1m away from x-directed electric Hertzian dipole with $\theta = 180°$ and $\phi = 90°$.

Magnetic Hertzian Dipole y—directed

Ex Field .1m from Dipole
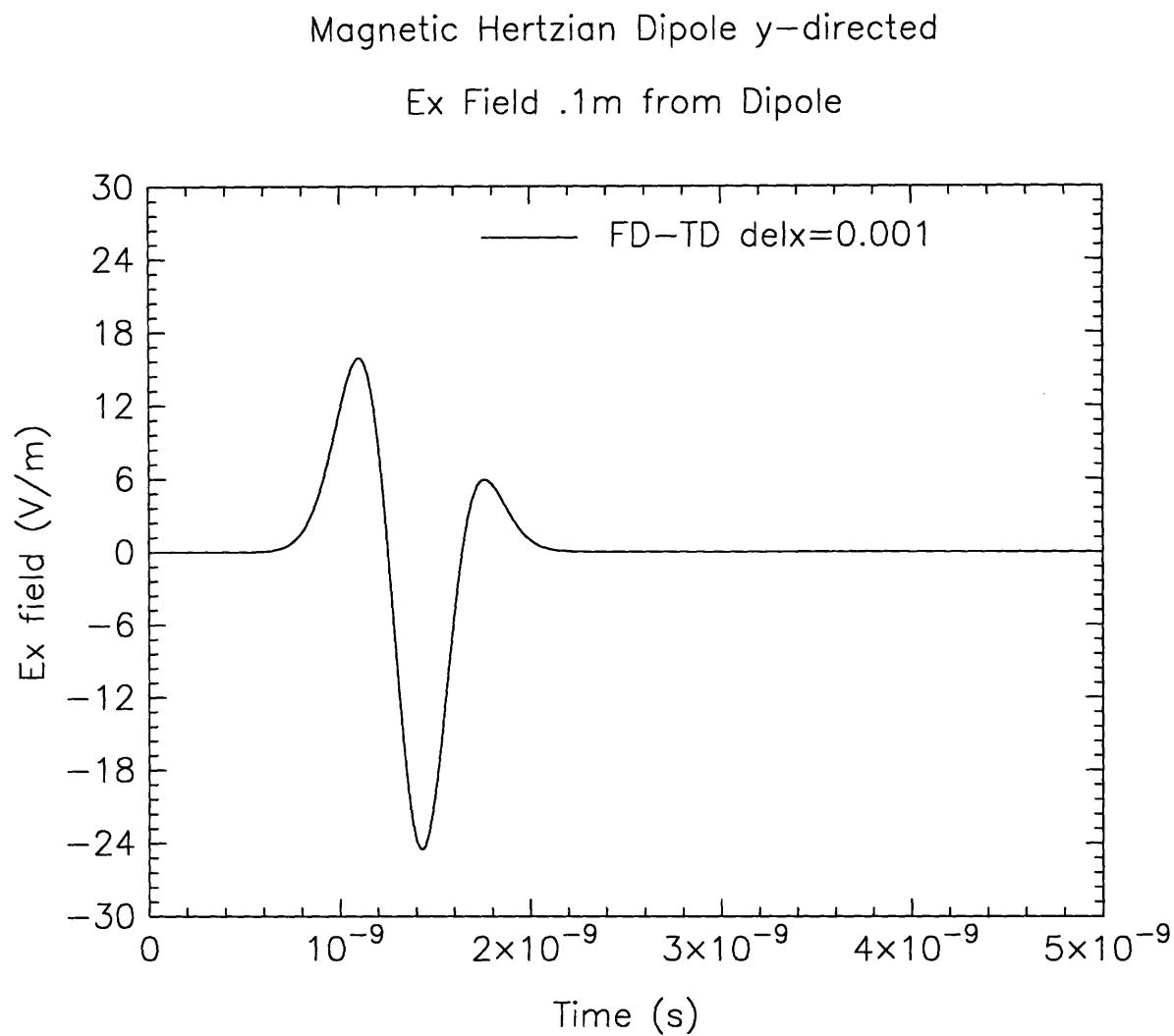
Figure 3.8: The Ex fields observed 0.1m away from y-directed magnetic Hertzian dipole with $\theta = 180°$ and $\phi = 0°$.

Chapter 4

Analytical Solution of Small Aperture

4.1   Introduction

It is possible to formulate an approximate analytical solution to the aperture problem solved by the Brute Force method in Chapter 3. This is important for verification and validation for both the Brute Force method and Induced Dipole method. The key to formulating an analytical solution is to use Babinet's principle to construct an equivalent problem as used in the Induced Dipole method, but instead of using the Finite Difference-Time Domain method to solve for the fields of dipoles we use the analytical solution of magnetic and electric dipoles. Since this analytical model for an infinite conducting plane with a single aperture uses electric and magnetic dipoles, the dipole fields from the FD-TD method (obtained in Chapter 3) will be compared to the analytical solution of the dipoles.

4.2   Electric Dipoles in Free Space

There is an analytical solution for the electric field of a Hertzian electric dipole [33], which can be derived using the dyadic Green's function $\overline{\overline{G}}(\vec{r},\vec{r}\,')$, given the current distribution $\vec{J}$.

This equation (4.1) is given below:

$$\bar{E}(\bar{r}) = i\omega\mu \iiint dv' \, \bar{\bar{G}}(\bar{r},\bar{r}') \cdot \bar{J}(\bar{r}')$$

(4.1)

where:

$$\bar{\bar{G}}(\bar{r},\bar{r}') = \left[\bar{\bar{I}} + \frac{1}{k^2}\nabla\nabla\right]\frac{e^{ik|\bar{r}-\bar{r}'|}}{4\pi|\bar{r}-\bar{r}'|}$$

(4.2)

For x-directed electric dipole, the current density is:

$$\bar{J}(\bar{r}') = \hat{x}Il\delta(\bar{r}')$$

(4.3)

The resulting E field from an x directed electric dipole is:

$$\bar{E}(\bar{r}) = -i\omega\mu Il\frac{e^{ikr}}{4\pi r}\left\{\hat{r}\left[\frac{i}{kr}+\left(\frac{i}{kr}\right)^2\right]2\sin\theta\cos\theta -\hat{\theta}\left[1+\frac{i}{kr}+\left(\frac{i}{kr}\right)^2\right]\cos\theta\cos\theta\right.$$
$$\left.+\hat{\phi}\left[1+\frac{i}{kr}+\left(\frac{1}{kr}\right)^2\right]\sin\theta\right\}$$

(4.4)

For normal incident $\phi = 90°$, and for propagation along the negative z-axis $\theta = 180°$, the above equations simplify to:

$$\bar{E}(\bar{r}) = -i\omega\mu Il\frac{e^{ikr}}{4\pi r}\left\{\hat{\phi}\left[1+\frac{i}{kr}+\left(\frac{i}{kr}\right)^2\right]\right\}$$

(4.5)

In applying Faraday's law $\bar{H} = \frac{1}{iw\mu}\nabla\times\bar{E}$ on equation (4.4) and using $\phi = 90°$ and

$\theta = 180°$, we obtain:

$$\bar{H}(\bar{r}) = ikIl\frac{e^{ikr}}{4\pi r}\left\{\hat{\theta}\left[1+\frac{i}{kr}\right]\right\}$$

(4.6)

Note: for $\phi = 90°$ and $\theta = 180°$

$$\overline{H}(\overline{r}) = H_y(r) = -ikIl\frac{e^{ikr}}{4\pi r}\left\{\left[1+\frac{i}{kr}\right]\right\} \tag{4.7}$$

Taking the inverse Fourier transform, we obtain:

$$H_y = \frac{l}{4\pi r}\left[\frac{1}{c}\frac{\partial}{\partial t}I\left(t-\frac{r}{c}\right)+\frac{1}{r}I\left(t-\frac{r}{c}\right)\right] \tag{4.8}$$

4.3   Magnetic Dipoles in Free Space

An analytical solution for a Hertzian magnetic dipole also can be constructed using (4.1) and applying the duality principal. For instance, to construct a y-directed Hertzian magnetic dipole, we first construct a y-directed Hertzian electric dipole as shown above for an x-directed electric dipole to obtain the E field, use Faraday's law to calculate the H field, and then apply duality to obtain a y-directed magnetic dipole's E field.

For a y-directed dipole the current density is: $\overline{J}(\overline{r}) = \hat{y}Il\delta(\overline{r})$ (4.9)

The resulting E field is:

$$\overline{E}(\overline{r}) = -i\omega\mu Il\frac{e^{ikr}}{4\pi r}\left\{\hat{r}\left[\frac{i}{kr}+\left(\frac{i}{kr}\right)^2\right]2\sin\theta\sin\phi-\hat{\theta}\left[1+\frac{i}{kr}+\left(\frac{i}{kr}\right)^2\right]\cos\theta\sin\phi\right.$$
$$\left.-\hat{\phi}\left[1+\frac{i}{kr}+\left(\frac{1}{kr}\right)^2\right]\cos\phi\right\} \tag{4.10}$$

For normal incident $\phi = 0°$, and for propagation along the z-axis $\theta = 180°$, the above equations simplify to:

$$\overline{E}(\overline{r}) = i\omega\mu Il\frac{e^{ikr}}{4\pi r}\left\{\hat{\phi}\left[1+\frac{i}{kr}+\left(\frac{i}{kr}\right)^2\right]\right\} \tag{4.11}$$

In applying Faraday's law $\overline{H} = \dfrac{1}{iw\mu}\nabla \times \overline{E}$ on equation (4.10) and using $\phi = 0°$ and

$\theta = 180°$, we obtain:

$$\overline{H}(\overline{r}) = -ikIl\frac{e^{ikr}}{4\pi r}\left\{\hat{\theta}\left[1+\frac{i}{kr}\right]\right\} \tag{4.12}$$

Using duality, we obtain:

$$\overline{E}(\overline{r}) = ikKl\frac{e^{ikr}}{4\pi r}\left\{\hat{\theta}\left[1+\frac{i}{kr}\right]\right\} \tag{4.13}$$

where: K is the magnetic current

Note: for $\phi = 0°$ and $\theta = 180°$

$$\overline{E}(\overline{r}) = E_x(r) = -ikKl\frac{e^{ikr}}{4\pi r}\left\{\left[1+\frac{i}{kr}\right]\right\} \tag{4.14}$$

Taking the inverse Fourier transform, we obtain:

$$E_x = \frac{l}{4\pi r}\left[\frac{1}{c}\frac{\partial}{\partial t}K\left(t-\frac{r}{c}\right)+\frac{1}{r}K\left(t-\frac{r}{c}\right)\right] \tag{4.15}$$

4.4   Analytical and FD-TD Dipole Results

The results using the analytical solution to Hertzian dipoles were obtained by providing a dipole moment, for electric dipole: Il and for magnetic dipole: Kl. For both the electric and magnetic dipole, the same dipole moment was used which was a doublet, the derivative of a Gaussian, as shown in Figure 2.3. This current is differentiated and multiplied by a constant -- the differentiate term is the far field and the constant term is the induction term.

For both the analytical and FD-TD (from Chapter 3) results, the distance between the dipole and observation point is 0.1m. From Figures 4.1 and 4.2, we see that both the

analytical and the FD-TD solutions are in perfect agreement. Thus, we have the confidence that the analytical solution and FD-TD solutions for both magnetic and electric dipoles are correct.

Electric Hertzian Dipole x—directed

Hy Field .1m from Dipole
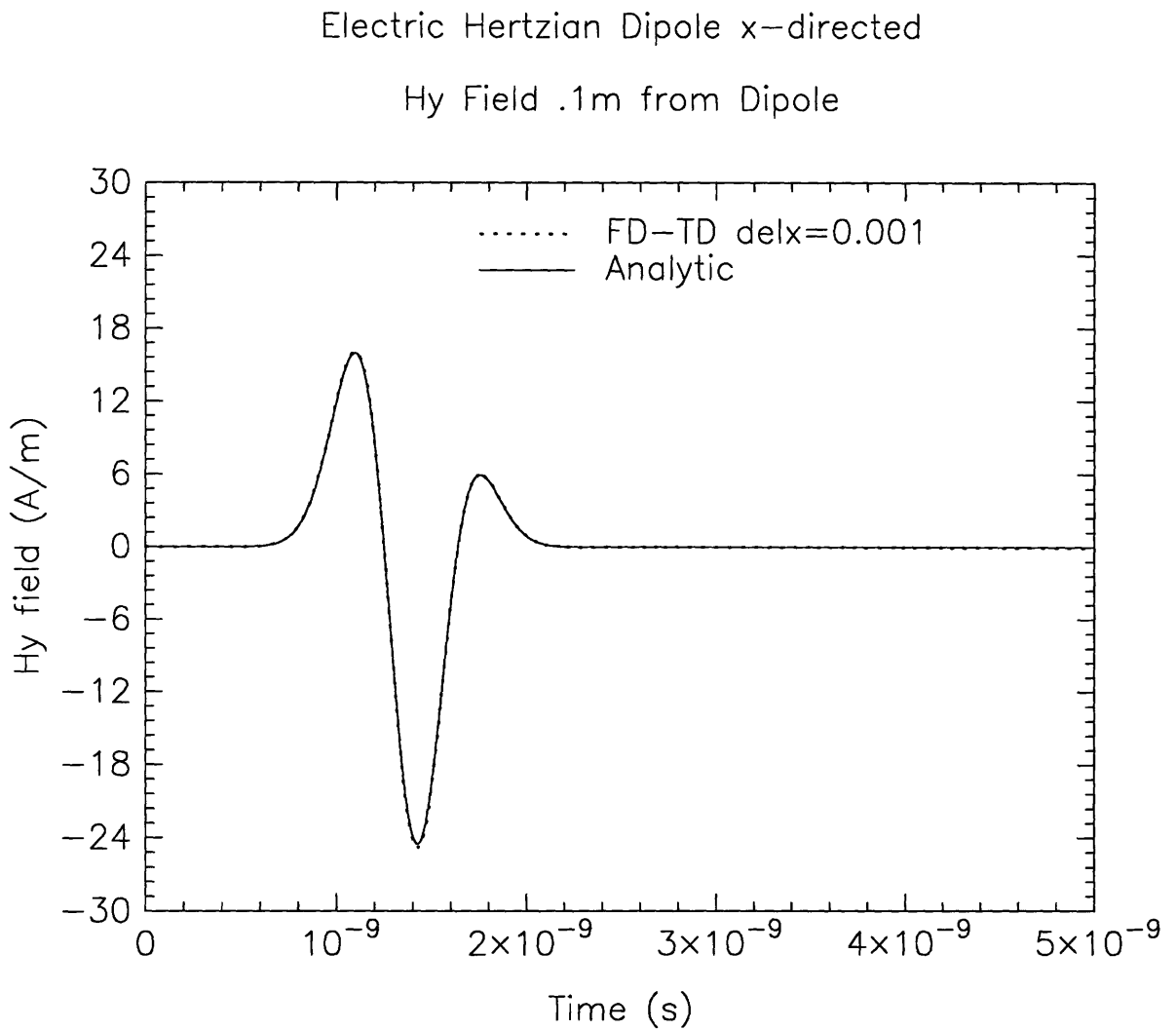

Figure 4.1: The Hy fields observed 0.1m away from x-directed electric Hertzian dipole with $\theta = 180°$ and $\phi = 90°$.

Magnetic Hertzian Dipole y—directed

Ex Field .1m from Dipole
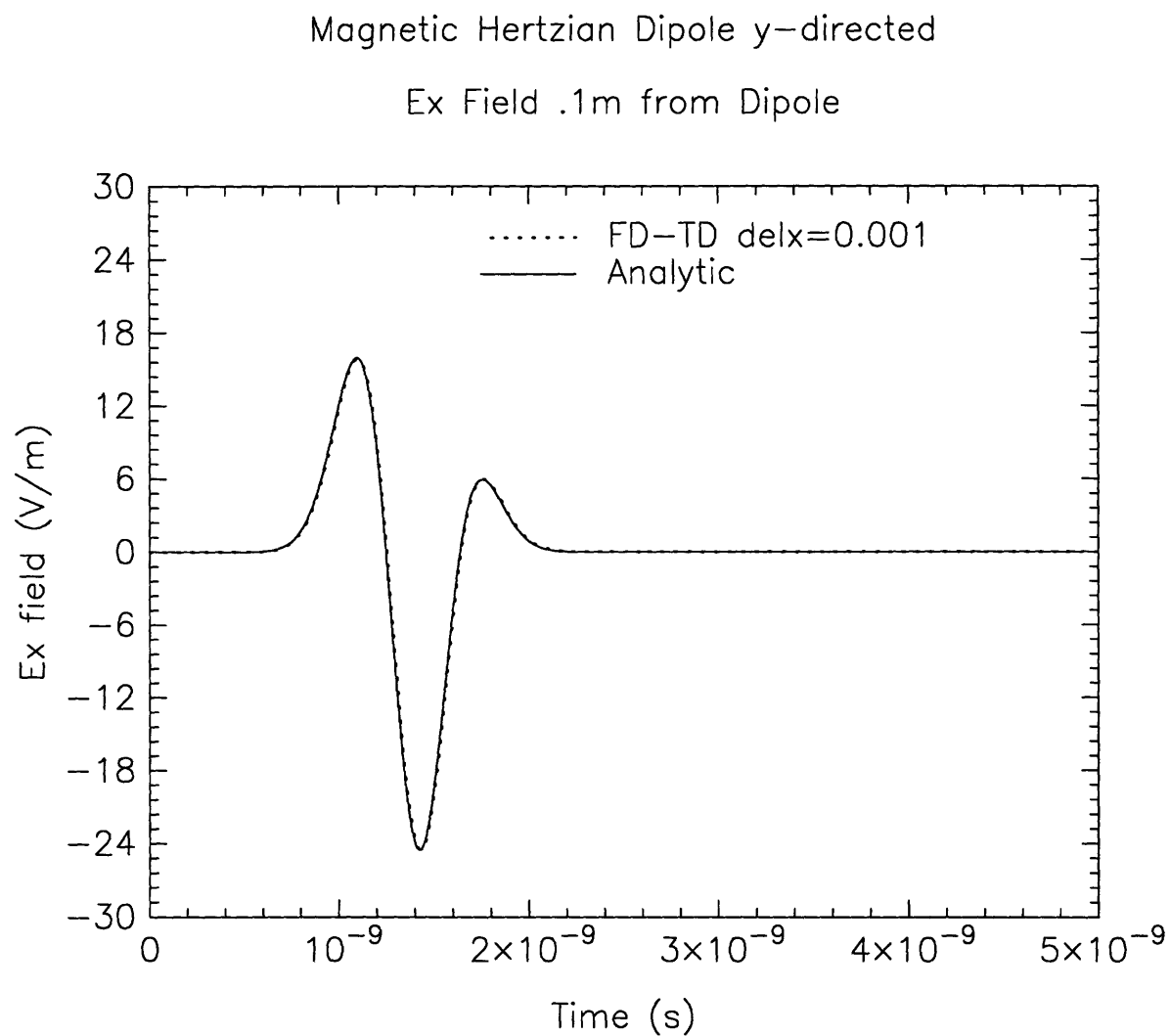
Figure 4.2: The Ex fields observed 0.1m away from y-directed magnetic Hertzian dipole with θ = 180° and φ = 0°.

4.5   Analytical Approximation to Aperture Problem

Since we now have analytical solutions for both electric and magnetic dipoles, we can formulate an analytical solution to the aperture problem described in Chapter 3. We start by applying the principles of the Induced Dipole method to obtain the induced dipoles which are described in Chapter 5.

From Chapter 5, the electric and magnetic current of the induced dipoles:

$$\eta I_z = -\frac{2a^3\eta_0}{3\Delta^2}\frac{\partial E_z^{sc}}{d\tau} \tag{4.16}$$

$$K_x = \frac{4a^3}{3\Delta^2}\eta\frac{dH_x^{sc}}{d\tau} \tag{4.17}$$

$$K_y = \frac{4a^3}{3\Delta^2}\eta\frac{\partial H_y^{sc}}{\partial\tau} \tag{4.18}$$

Since x-directed electric dipole is the excitation source at normal incidence and propagation along the negative z-axis, only two fields are observed H_y and E_x. From the above equations, we can see that only one induced dipole is induced, namely y-directed magnetic dipole with magnetic current K_y. Note that the currents are in terms of the short circuit field, not normally known. This short circuit field is produced when the aperture is shorted resulting in a solid infinite ground plane. The total field is composed of the short circuit fields and field scattered by the aperture. For small apertures, the field scattered by the aperture is negligible, thus it can be ignored, while still producing extremely accurate results. The relationship between the incident field and short circuit fields are as follows:

$$\frac{\partial E_x^{sc}}{\partial z} = 2\frac{dE_x^i}{dz} \tag{4.19}$$

$$\frac{\partial E_y^{sc}}{\partial z} = 2\frac{\partial E_y^i}{\partial z} \tag{4.20}$$

$$E_z^{sc} = 2E_z^i \tag{4.21}$$

The above equations result from having radiating fields in the presence of an infinite conducting plane. Using the Induced Dipole technique, another induced dipole is placed on the other side of the infinite conducting plane, but opposite in direction to the original induced dipole (see Figure 4.3). The infinite conducting plane actually decouples the aperture problem into two separate problems. One problem is the generation of the original induced dipole; the other problem is the oppositely opposed induced dipoles. In both cases, the fields are radiating in the presence of the infinite conducting plane, which means that the induced magnetic current for our case must be multiplied by a factor of 4. A factor of 2 is introduced by each of the decoupled problems. Thus, the analytical equation for the magnetic current of the induced dipole becomes:

$$K_y = 4 \frac{4a^3}{3\Delta^2} \eta \frac{\partial H_y^i}{\partial \tau} \tag{4.22}$$

Note that for the analytical formulation there is an extra factor of 4 introduced because the aperture decouples into separate problems which have to be simulated by using boundary conditions of infinite conducting plane. In the FD-TD method, the infinite conducting plane we define automatically introduces this factor of 4 because the FD-TD method used is a total field solver.

$$\overline{H}^{total} = \overline{H}^{sc} + \overline{H}^{ap} \tag{4.23}$$

where,
$$\overline{H}^{sc} = \overline{H}^r + \overline{H}^i \tag{4.24}$$

$\overline{H}^{sc}$: is the short circuit H field

$\overline{H}^{ap}$: is the H field scattered by the aperture

$\overline{H}^r$: is reflected H field due to infinite conducting plane

$\overline{H}^i$: is the incident H field

for small aperture $\overline{H}^{ap} = 0$, so

$$\overline{H}^{total} = \overline{H}^{sc} \tag{4.25}$$

Putting it all together, we get:

$$H_y^i = \frac{l}{4\pi r_{da}}\left[\frac{1}{c}\frac{\partial}{\partial t}I\left(t - \frac{r_{da}}{c}\right) + \frac{1}{r_{da}}I\left(t - \frac{r_{da}}{c}\right)\right] \tag{4.26}$$

$$K_y = 4\frac{4a^3}{3\Delta^2}\eta\frac{\partial H_y^i}{\partial \tau} \tag{4.27}$$

$$E_x = \frac{l}{4\pi r_{ao}}\left[\frac{1}{c}\frac{\partial}{\partial \tau}K_y\left(t - \frac{r_{ao}}{c}\right) + \frac{1}{r_{ao}}K_y\left(t - \frac{r_{ao}}{c}\right)\right] \tag{4.28}$$

Given a current I, use equation (4.26) to obtain incident H field H_y^i. Then, calculate the induced magnetic current K_y (4.27). Use the induced magnetic current for the magnetic dipole, which generated the observed E field E_x. This is how the aperture problem is solved analytically.
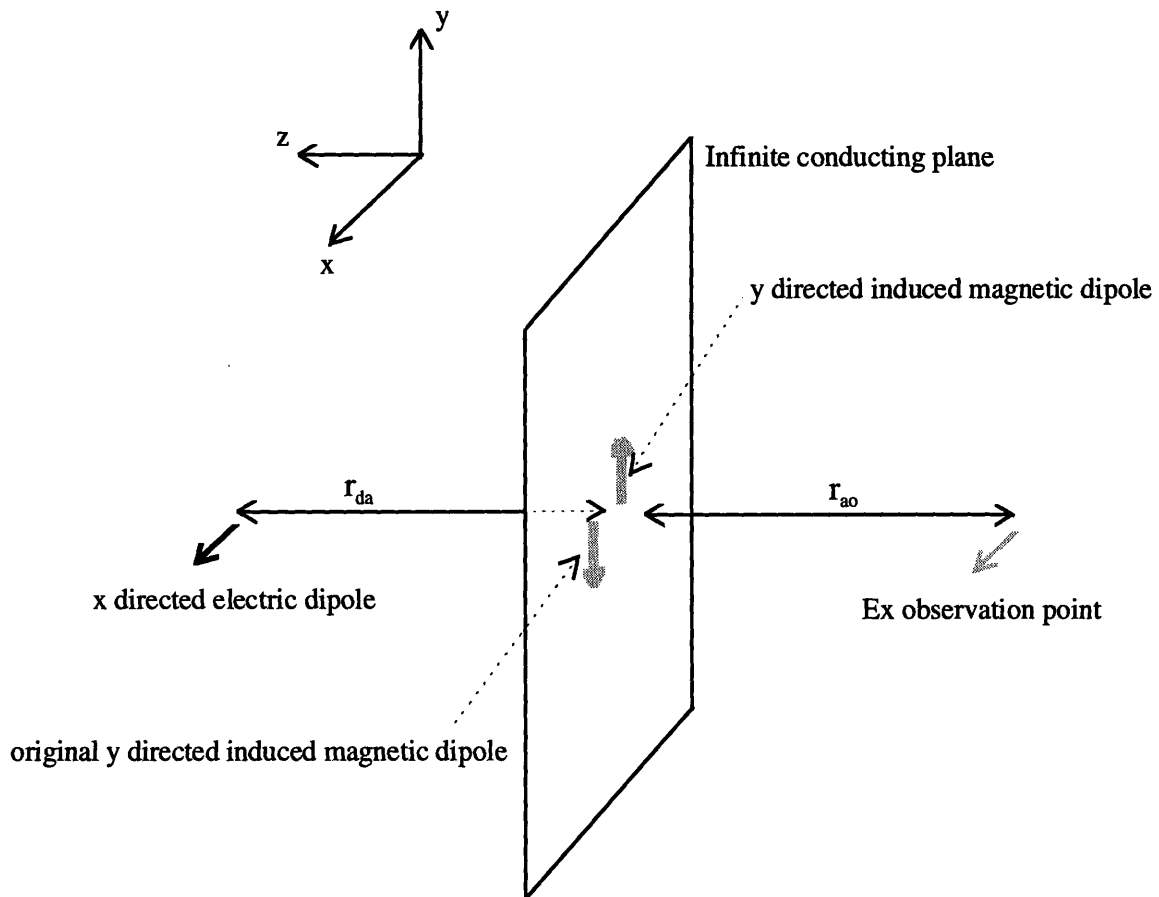
Figure 4.3: Induced Dipole method excited by an x-directed electric dipole with the observation point at normal incidence along the negative z axis.

4.6   Comparison of Brute Force to Analytical Solution

In Figure 4.4 and Figure 4.5, the results of solving the aperture problem using an approximate analytic solution is compared to the results obtained using the Brute Force method. From Figures 4.4 and 4.5, we see that the Brute Force method overestimates the observed field by over 50%. The main reasons that the Brute Force method overestimates the observed field are due to the staircasing of the circular aperture as shown in Figure 3.1 and to the staircased aperture which is slightly larger in area. The Brute Force simulations were performed with an aperture of 80 cells which is not enough cells to provide the resolution required to obtain accurate results. If the aperture in the Brute Force method were represented with more than 80 cells, the error would be decreased as the number of cells used to represent the aperture increased. Increasing the number of cells reduces the error due to staircasing by more accurately representing a perfect circle and matching the area of the perfect circle (78.54 mm^2) to that of a staircased circular aperture with 80 cells (80.0 mm^2). Due to computer memory restrictions, the circular aperture could not be represented with more than 80 cells.

Brute Force vs Analytical Solution

Ex Field .1m from Aperture

Figure 4.4: FD-TD simulation of an infinite ground plane with an aperture of radius 0.005m using the Brute Force method compared to the analytical solution. The excitation source is 0.1m away from the aperture and the observation point is also 0.1m away.

Brute Force vs Analytical Solution

Ex Field .1m from Aperture

Figure 4.5: Frequency domain results of FD-TD simulation of an infinite ground plane with an aperture of radius 0.005m using the Brute Force method compared to the analytical solution. The excitation source is 0.1m away from the aperture and the observation point is also 0.1m away.

In Figures 4.6 and 4.7, the Brute Force method with an aperture of radius 5.0mm is compared to that of an aperture of radius 5.7mm using the analytical solution. These figures show that by increasing the radius of the aperture in the analytical solution, the Brute Force method with an aperture with radius of 5.0mm and 80 cells matches the approximate analytical solution with a radius of 5.7mm. It can be inferred that the Brute Force method yields results of a slightly larger aperture of radius 5.7mm instead of a radius 5.0mm. By increasing the radius of the aperture in the analytical solution to 5.7mm, we were able to compensate for the staircasing error in the Brute Force method which caused the inaccurate larger observed fields as shown in Figures 4.4 and 4.5.

Clearly, a better method that is more efficient and does not introduce staircasing error is necessary to solve this aperture problem. The next chapter will describe such a method; it is the Induced Dipole method.
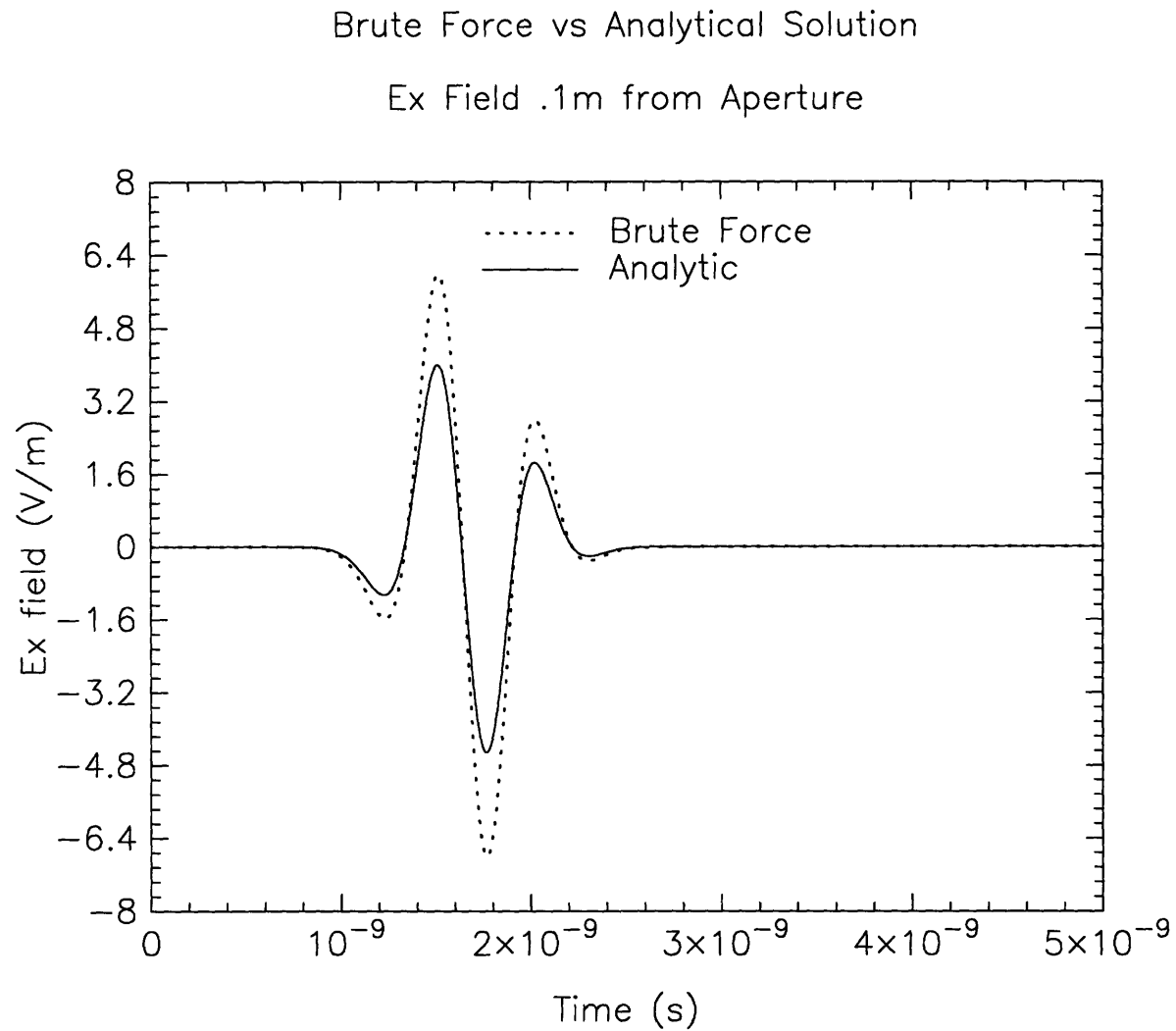
Figure 4.6: FD-TD simulation of an infinite ground plane with an aperture of 0.005m using the Brute Force method compared to the analytical solution with an aperture of 0.0057m. The excitation source is 0.1m away from the aperture and the observation point is also 0.1m away.

Calibrated Brute Force vs Analytical Solution

Ex Field .1m from Aperture
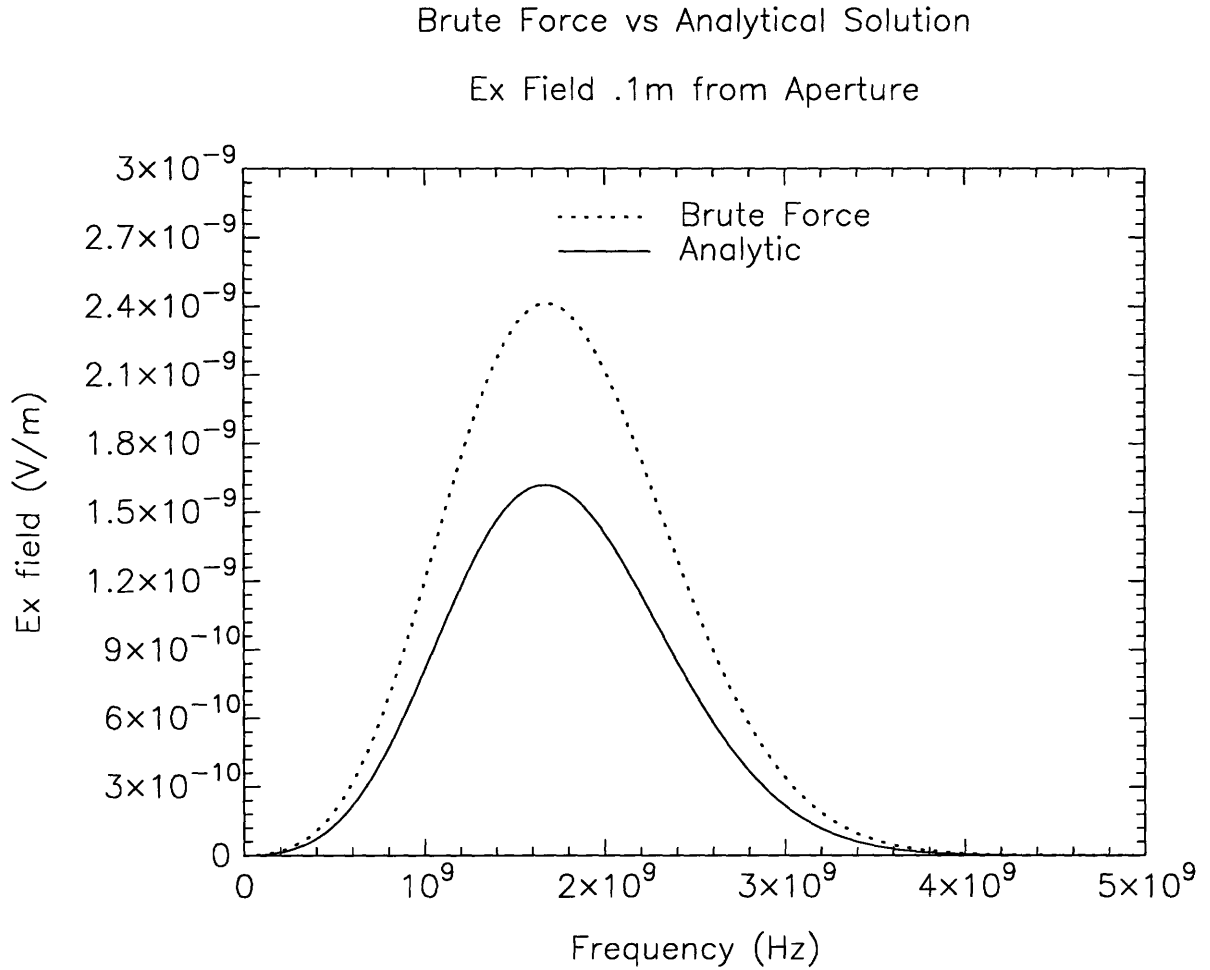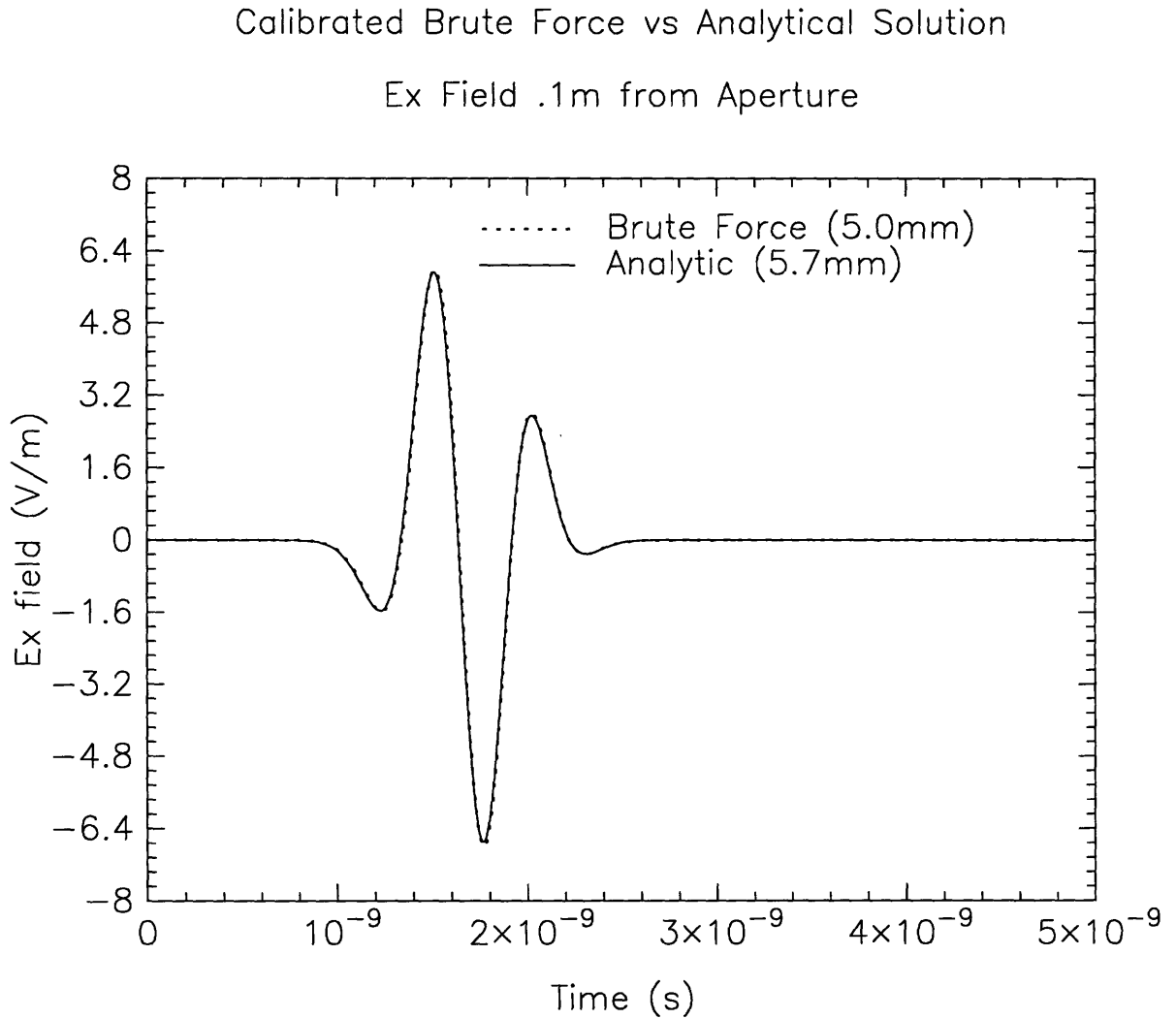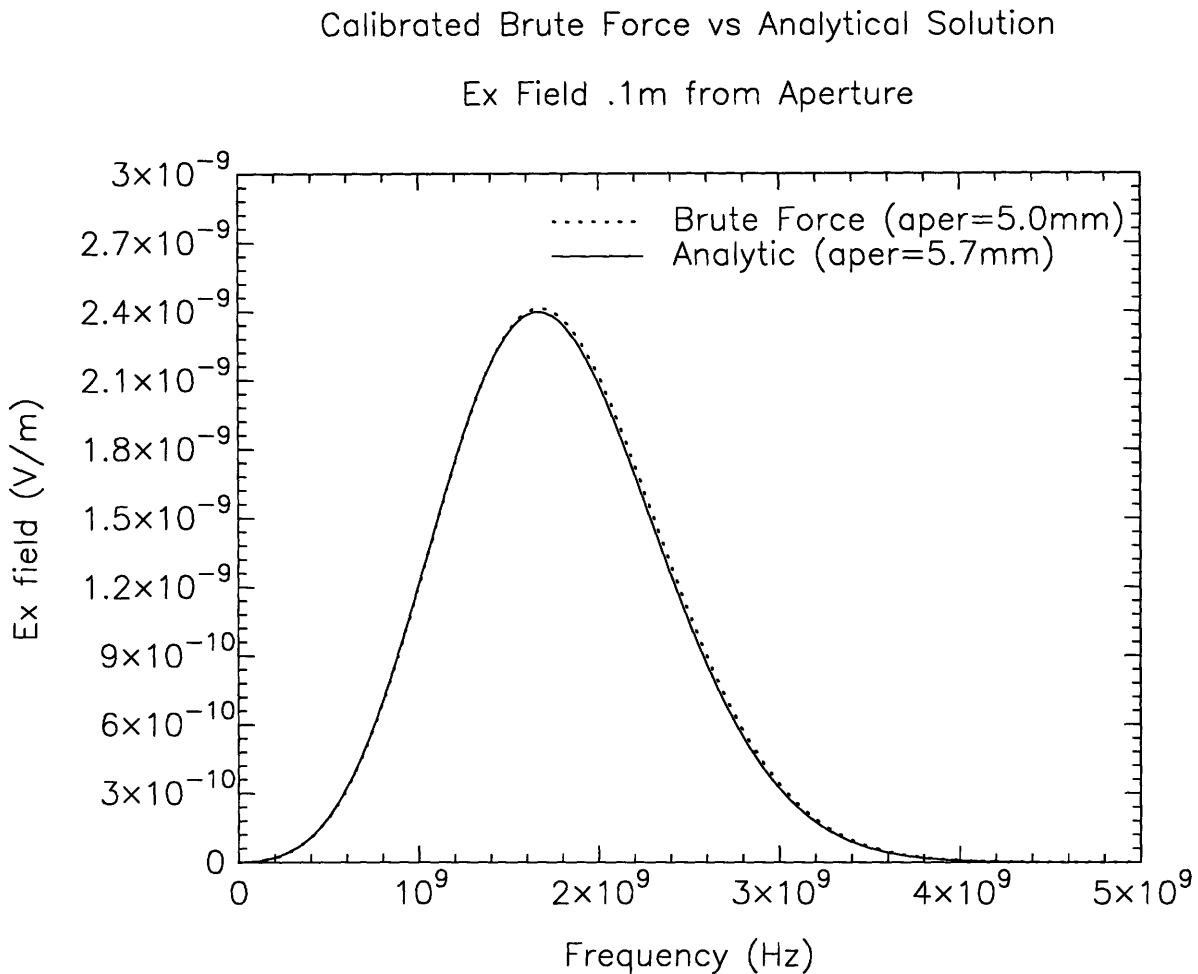

Figure 4.7: Frequency domain results of FD-TD simulation of an infinite ground plane with an aperture of 0.005m using the Brute Force method compared to the analytical solution with an aperture of 0.0057m. The excitation source is 0.1m away from the aperture and the observation point is also 0.1m away.

Chapter 5

Induced Dipole Method

5.1 Formulation

In Chapter 4, it was shown that the Brute Force technique could solve the aperture problem described, but it was far too inefficient to solve electrically small apertures. The Induced Dipole method can efficiently solve this aperture problem with extreme accuracy. My implementation of the Induced Dipole method will build on the work conducted by Oates on small round apertures, which are much smaller than one spatial cell, by using the Liao absorbing boundary condition to increase accuracy by minimizing the reflections due to the boundary conditions. In addition, the excitation source used for the aperture problem is a Hertzian dipole, instead of a plane wave as used by Oates. A Hertzian dipole excitation more accurately models the sources found in electronics. The small round aperture is modeled by a pair of oppositely directed electric dipoles with the same electric current moment (5.1) and a pair of oppositely directed magnetic dipoles with the same magnetic current moments, (5.2) and (5.3). The pair of oppositely opposed magnetic and electric dipoles replace the round aperture by being placed on either side of the aperture, then shorting the aperture.

$$\eta I_z^n (l,m,0) = -\frac{2a^3 \eta_0}{3\Delta^2} [h_y^{n-1}(l,m,0) - h_y^{n-1}(l-1,m,0) + h_x^{n-1}(l,m-1,0) - h_x^{n-1}(l,m,0)] \qquad (5.1)$$

$$K_x^n(l,m,0) = \frac{4a^3}{3\Delta^2}[e_y^n(l,m,1) - e_z^n(l,m+1,0) + e_z^n(l,m,0)] \tag{5.2}$$

$$K_y^n(l,m,0) = \frac{4a^3}{3\Delta^2}[e_x^n(l,m,1) - e_z^n(l,m,0) + e_z^n(l+1,m,0)] \tag{5.3}$$

The above electric current and magnetic current can be related to current densities used in the Finite Difference-Time Domain equations (2.15) to (2.20), using the following equations:

$$I = J_e \cdot \Delta^2 \tag{5.4}$$

$$K = J_m \cdot \Delta^2 \tag{5.5}$$

where, Δ can be approximated by using the corresponding discretization length.

As shown in Chapter 4, the short circuit field is approximated by the total field which induces a small error. This error can be eliminated by subtracting the field produced by the induced electric and magnetic dipoles as shown by Oates [12]. The resulting induced electric and magnetic currents are the following:

$$\eta I_z^n = [1 + \alpha_1(\frac{a}{\Delta})^3]\eta\tilde{I}_z^n + \alpha_3(\frac{a}{\Delta})^3(\tilde{K}_x^n - \tilde{K}_x^{n-1}) \tag{5.6}$$

$$K_x^n = \alpha_2(\frac{a}{\Delta})^3(\eta\tilde{I}_z^n - \eta\tilde{I}_z^{n-1}) + [1 - \alpha_4(\frac{a}{\Delta})^3]\tilde{K}_x^n + \alpha_5(\frac{a}{\Delta})^3\tilde{K}_y^n) \tag{5.7}$$

$$K_y^n = -\alpha_2(\frac{a}{\Delta})^3(\eta\tilde{I}_z^n - \eta\tilde{I}_z^{n-1}) + [1 - \alpha_4(\frac{a}{\Delta})^3]\tilde{K}_y^n + \alpha_5(\frac{a}{\Delta})^3\tilde{K}_x^n) \tag{5.8}$$

Note: $\eta\tilde{I}_n$, $\tilde{K}_x$, and $\tilde{K}_y$ are the uncorrected currents (5.1) - (5.3).

where,

$$\alpha_1 = \frac{8\gamma_e\sigma_1}{\pi^2} \tag{5.9}$$

$$\alpha_2 = \frac{2\gamma_m \sigma_1}{\pi^2}\left(\frac{\Delta}{\Delta\tau}\right) \tag{5.10}$$

$$\alpha_3 = \frac{4\gamma_e \sigma_2}{\pi^2}\left(\frac{\Delta}{\Delta\tau}\right) \tag{5.11}$$

$$\alpha_4 = \frac{8\gamma_m \sigma_3}{\pi^2} \tag{5.12}$$

$$\alpha_5 = \frac{8\gamma_m \sigma_4}{\pi^2} \tag{5.13}$$

where,
$$\gamma_e \equiv \frac{\alpha_e}{a^3} \quad \text{and} \quad \gamma_m \equiv \frac{\alpha_m}{a^3} \tag{5.14}$$

$$\alpha_e \equiv \frac{2a^3}{3} \quad \text{and} \quad \alpha_m \equiv \frac{4a^3}{3}$$

The constants below were evaluated using Simpson's rule [12].

$$\sigma_1 \equiv \int_0^{\frac{\pi}{2}} dx \int_0^{\frac{\pi}{2}} dy \left\{ \sqrt{(\sin^2 x + \sin^2 y)(1 + \sin^2 x + \sin^2 y)} - (\sin^2 x + \sin^2 y) \right\} \tag{5.15}$$

$$\sigma_1 = 0.9753582$$

$$\sigma_2 \equiv \int_0^{\frac{\pi}{2}} dx \int_0^{\frac{\pi}{2}} dy \frac{\sin^2 y \cos^2 x}{\sqrt{(1 + \sin^2 x + \sin^2 y)}} = 0.4877207 \tag{5.16}$$

$$\sigma_3 \equiv \int_0^{\frac{\pi}{2}} dx \int_0^{\frac{\pi}{2}} dy \sqrt{\frac{\sin^2 x + \sin^2 y}{1 + \sin^2 x + \sin^2 y}} \cos^2 x = 0.7466728 \tag{5.17}$$

$$\sigma_4 \equiv \int_0^{\frac{\pi}{2}} dx \int_0^{\frac{\pi}{2}} dy \frac{\sin^2 x \sin^2 y}{\sqrt{\sin^2 x + \sin^2 y}} \left\{ \sqrt{1 + \sin^2 x + \sin^2 y} - \sqrt{\sin^2 x + \sin^2 y} \right\} \tag{5.18}$$

$$\alpha_4 = 0.1913744$$

The above induced electric and magnetic currents will be used as currents for the electric and the magnetic induced dipoles. It is these induced dipoles which will be used to model an electrically small aperture.

As shown in Chapter 4 - Figure 4.3, the Induced Dipole method is implemented by first shorting the aperture so that the infinite plane is solid without any holes. Then, electric and magnetic induced dipoles are placed on the excitation side (the side where the excitation source is located) as given by the induced magnetic and electric currents provided above. These same induced dipoles are placed on the observation side of the aperture, but are oppositely opposed to the original dipoles so that dipoles are oppositely directed. The main advantage to this method is that it provides very accurate results without finely gridding the computational domain.

5.2 Induced Dipole Results

In Figures 5.1 and 5.2, the Induced Dipole method, using various scaling factors, is compared to the analytical solution in the time and frequency domain, respectively. The scaling factor describes how large each dimension of a gridding cube of the Induced Dipole method is compared to each dimension of a gridding cube of the Brute Force method. For instance, a scaling factor of 10 means that for the Induced Dipole simulation, the x, y, and z dimensions of a Induced Dipole gridding cube is 10 times larger than the Brute Force gridding cube. For uniform gridding ($\Delta x = \Delta y = \Delta z$), that essentially means that the same computational domain in physical dimensions has 1000 times less cubes in the Induced Dipole method than in the Brute Force method. For my simulations, the Brute Force method contains cubes of size: $\Delta x = \Delta y = \Delta z = 0.001$m; for the Induced Dipole method with a scaling factor of 10, $\Delta x = \Delta y = \Delta z = 0.01$m. As shown in Figures 5.1 and 5.2, the Induced Dipole method provides very accurate results compared to the analytical solution for various scaling factors. Note that the larger the scaling factor, the larger the gridding cubes, which translates to a FD-TD problem that requires much less memory and computer time to solve. Scaling factors larger than 16.6 or smaller than 8.33 produce results which are less accurate.

Figure 5.3 shows the percent of error for the Induced Dipole method using various scaling factors compared to the analytical solution in the frequency domain. In the region of interest, the resonance, the Induced Dipole method produces results within 5% of the analytical solution.

Figure 5.1: FD-TD simulations using the Induced Dipole method (using various scaling factors) compared to the analytical solution.
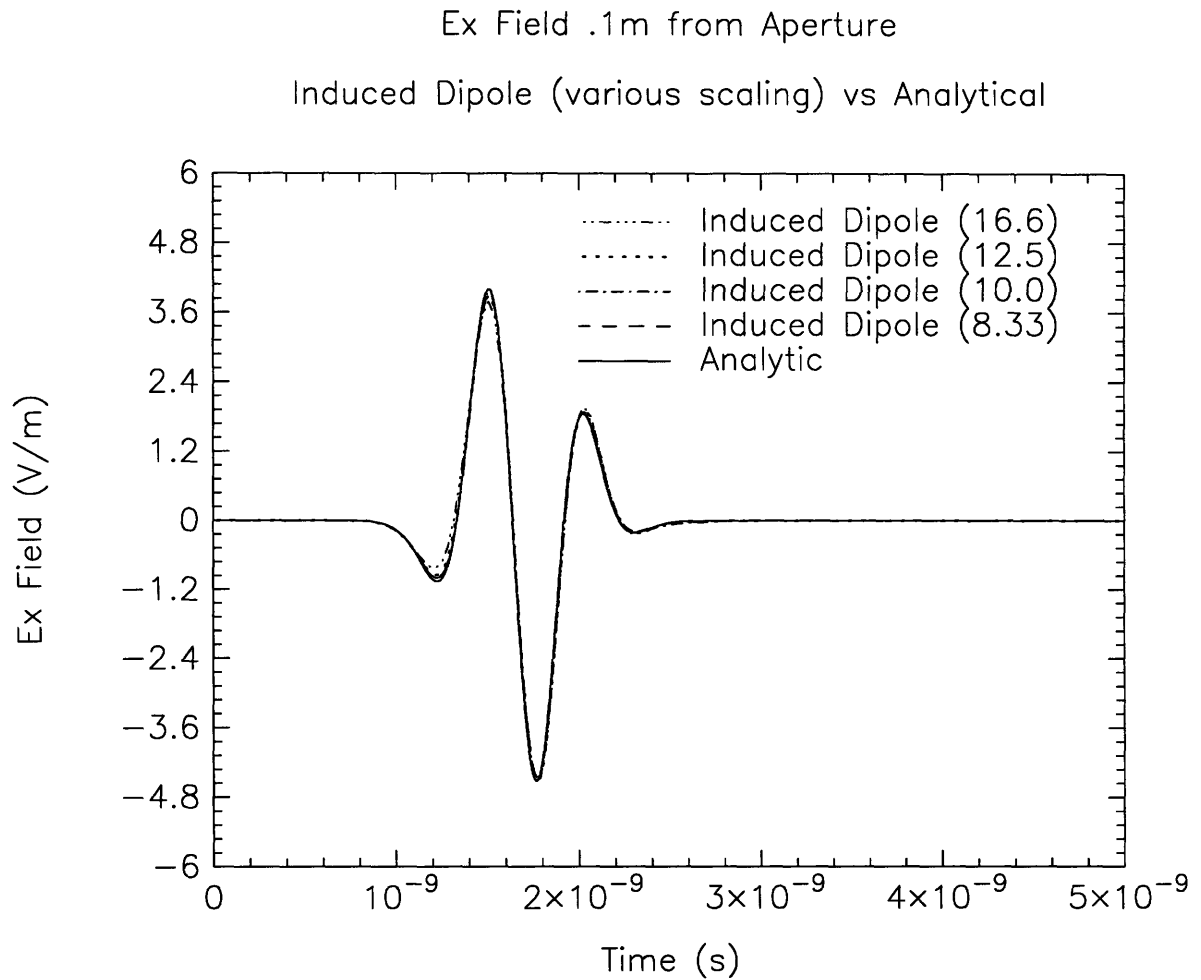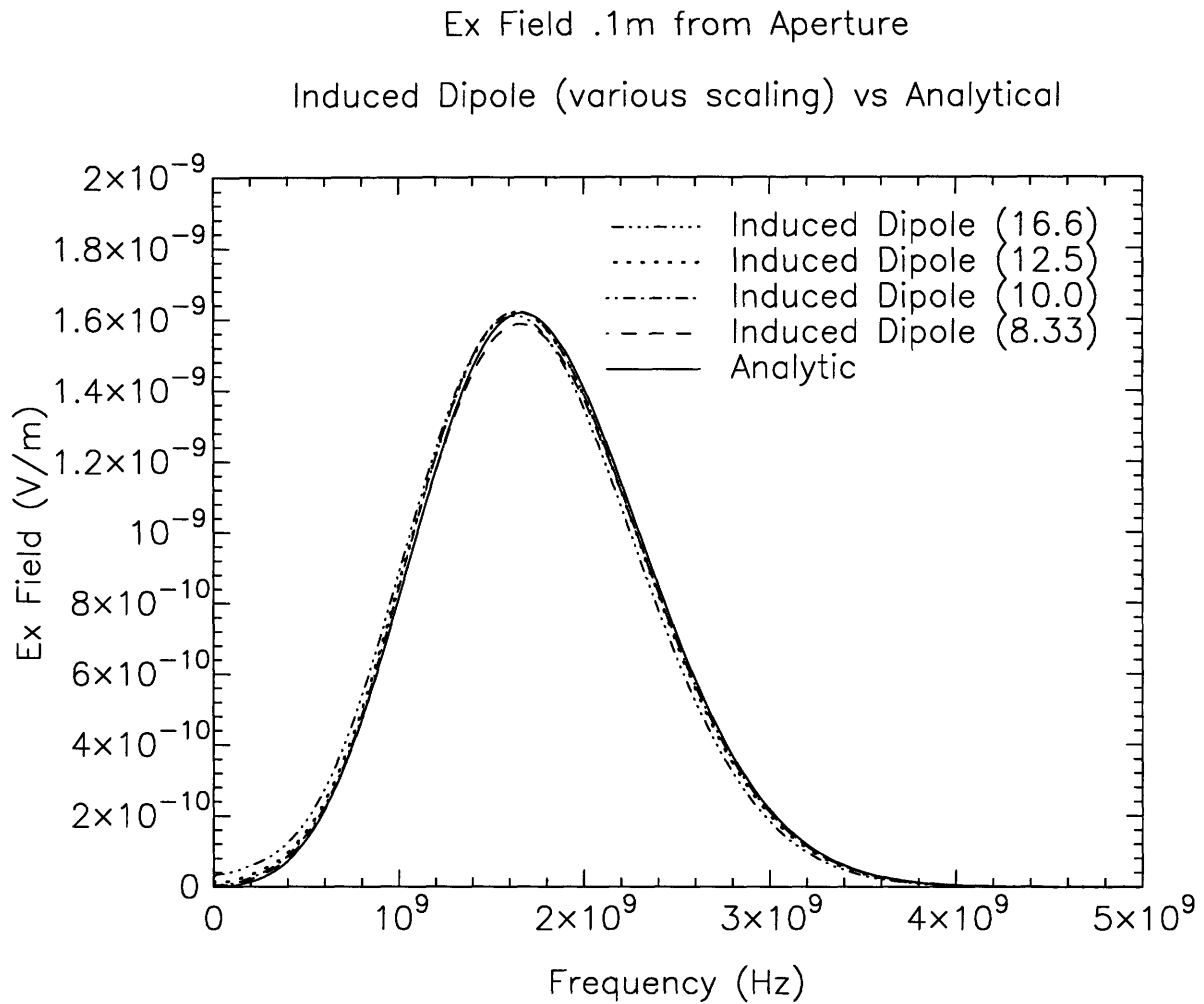
Figure 5.2: Frequency domain results of FD-TD simulations using the Induced Dipole method (using various scaling factors) compared to the analytical solution.
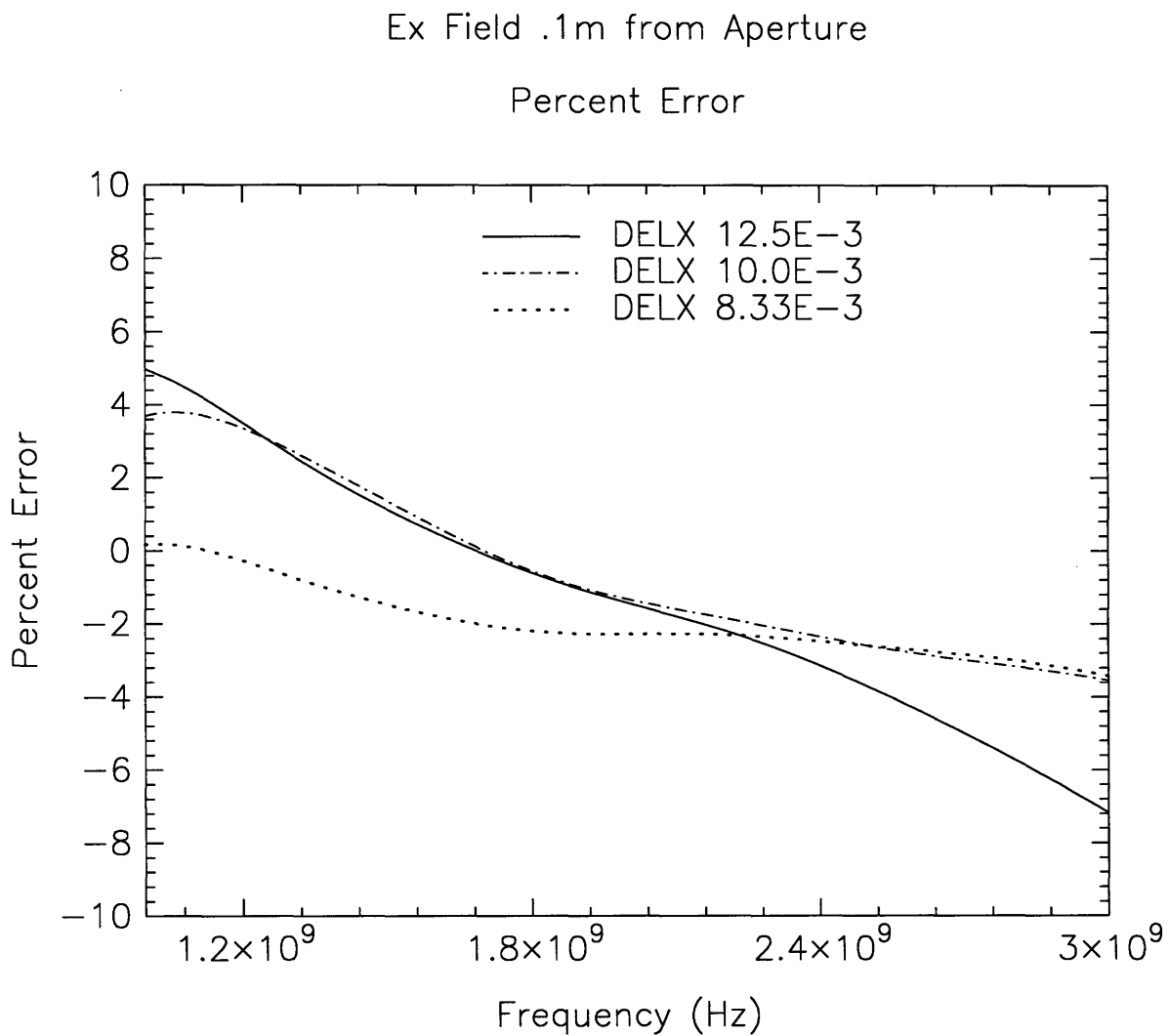
Ex Field .1m from Aperture

Percent Error

Figure 5.3: Percent error of Induced Dipole method of various scaling factors with respect to the analytical solution.

Chapter 6

Summary and Conclusions

The problem of modeling a small circular aperture using the Finite Difference-Time Domain method was solved using two methods: 1) Induced Dipole method and 2) Brute Force method. Both methods were compared to an approximate analytical solution. The Induced Dipole method was shown to produce superior results to those produced by the Brute Force method.

In our aperture problem (Figure 3.2) where we have an infinite metal plate with an aperture of radius 0.005m and $r_{da} = r_{ao} = 0.1m$, we obtain the results shown in Figures 6.1 and 6.2 using the Brute Force method, Analytical method, and Induced Dipole method. From Figures 6.1 and 6.2, we see that the Brute Force method overestimates the radiation from the apertures by over 50%, thus the Brute Force cannot be depended upon to provide accurate results without increasing the gridding finer than 0.001m to reduce the staircasing error. On the other hand, the Induced Dipole method provides results that are within 5% in the 1 to 3 GHz frequency region where most of the spectral energy is concentrated. Furthermore, at the resonance frequency 1.6 GHz, the error produced by the Induced Dipole method is within 2% of the analytical solution. This method produces results which are very accurate, by using about 1000 times less memory and running about 1000 times faster than the Brute Force method (depending on the scaling factor used).
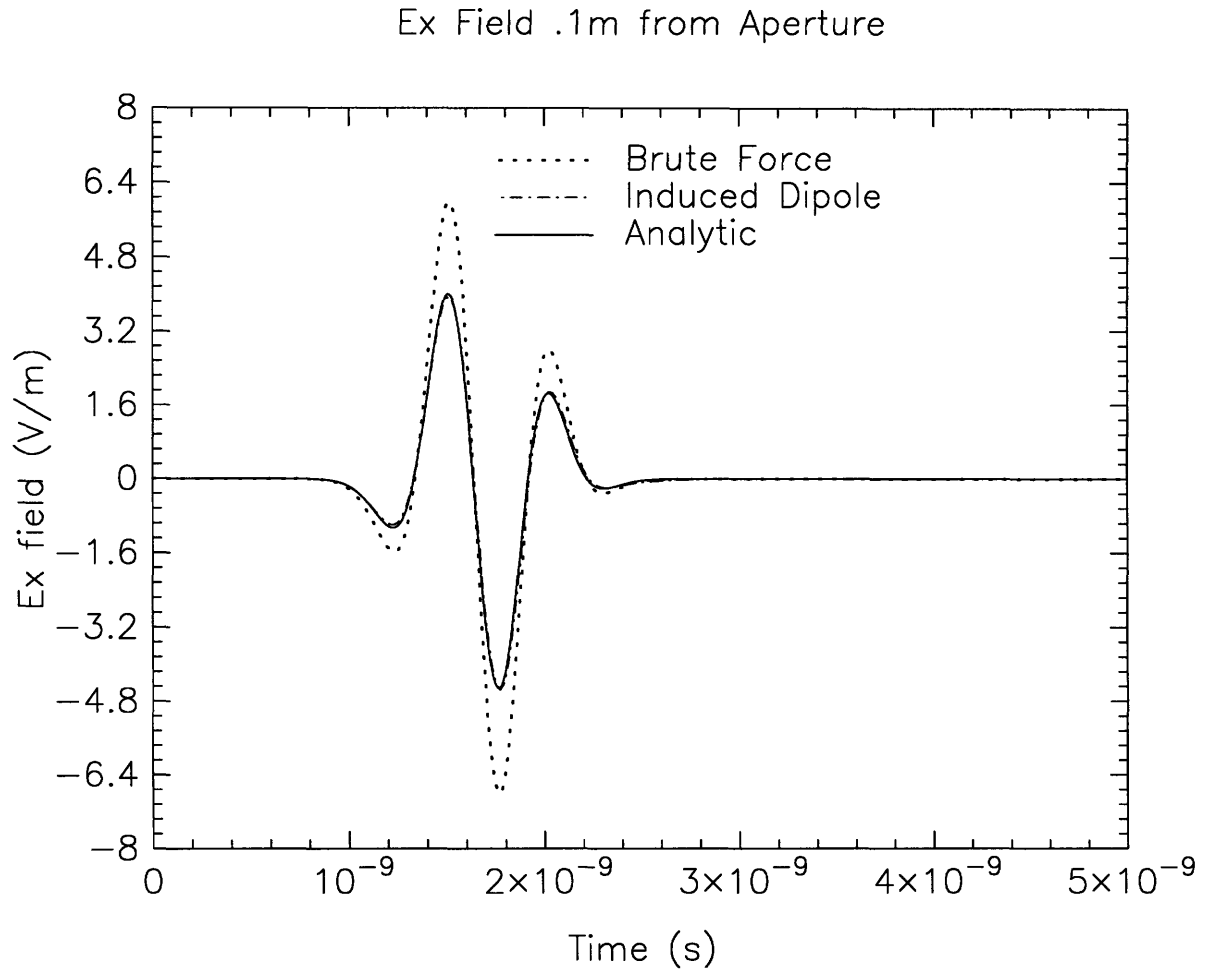
Ex Field .1m from Aperture

Figure 6.1: Time Domain comparison of Brute Force method and Induced Dipole method with respect to the analytical solution.

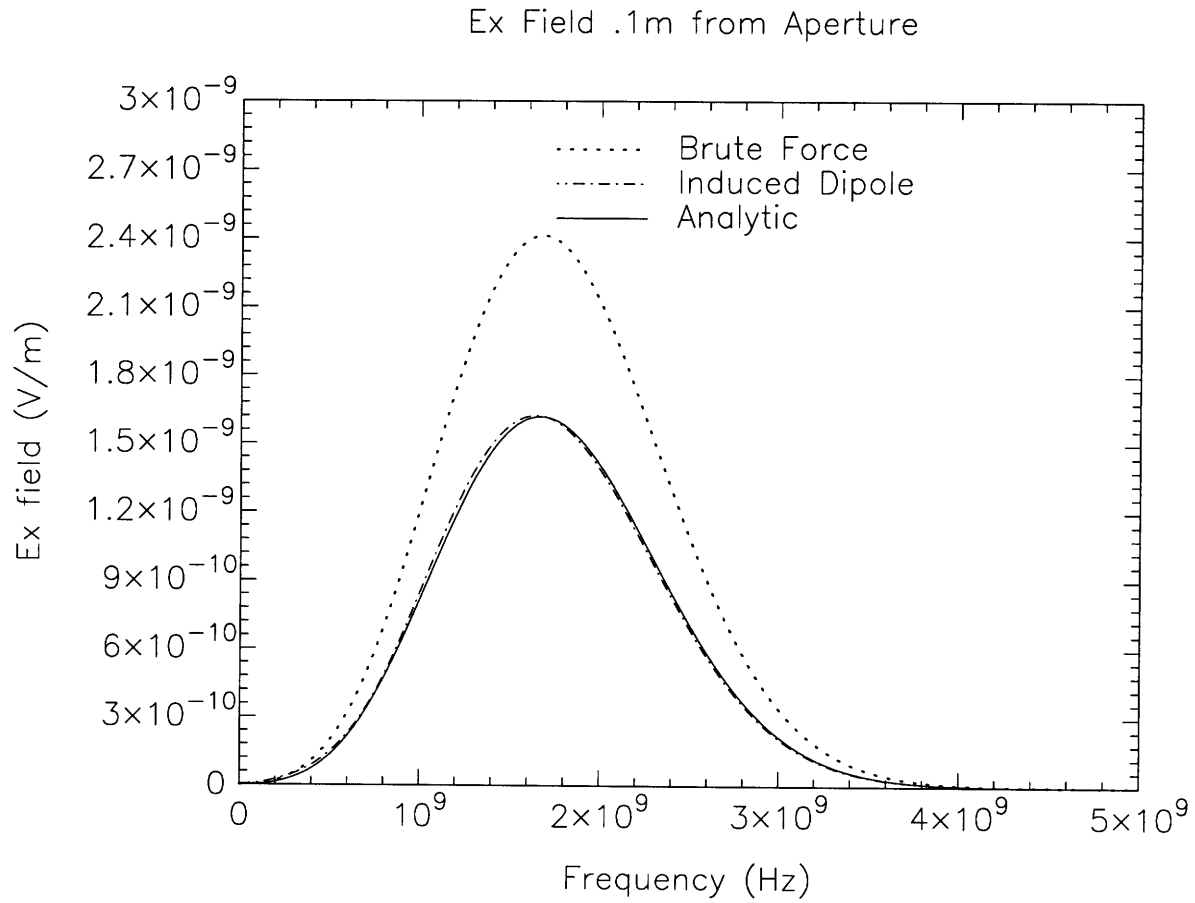Figure 6.2: Frequency domain comparison of Brute Force method and Induced Dipole method with respect to the analytical solution.

References

[1]   H. W. Ott, *Noise Reduction Techniques in Electronic Systems*, 2nd Edition, New York, Wiley and Sons, 1988. H. W. Ott, *Noise Reduction Techniques in Electronic Systems*, 2nd Edition, New York, Wiley and Sons, 1988.

[2]   J. Gilbert, R. Holland, "Implementation of the Thin-Slot Formalism in the Finite-Difference EMP Code THREDII," IEEE Tran. Nuc. Sci., Vol. NS-28, No. 6, pp. 4269-4274, Dec. 1981.

[3]   C. D. Turner, L. D. Bacon, "Evaluation of a Thin-Slot Formalism for Finite-Difference Time-Domain Electromagnetic Codes," IEEE Trans. Electromag. Comp., Vol. 30, No. 4, pp. 523-528, Nov. 1988.

[4]   D. J. Riley, C. D. Turner, "Hybrid Thin-Slot Algorithm for the Analysis of Narrow Apertures in Finite-Difference Time-Domain Calculations," IEEE Trans. Antennas and Prop., Vol. 38, No. 12, pp. 1943-1950, Dec. 1990.

[5]   K. R. Demarest, "A Finite Difference-Time Domain Technique for Modeling Narrow Apertures in Conducting Scatterers," IEEE Trans. Antennas and Prop., Vol. AP-35, No. 7, pp. 826-831, July 1987.

[6]   A. Taflove, K Umashankar, "A Hybrid Moment Method/Finite-Difference Time-Domain Approach to Electromagnetic Coupling and Aperture Penetration into Complex Geometries," IEEE Trans. Antennas and Prop., Vol. AP-30, No. 4, pp. 617-627, July 1982.

[7]   A. Taflove, K. R. Umashankar, F. Harfoush, B. Beker, F. Harfoush, and K. S. Yee, "Detailed FD-TD Analysis of Electromagnetic Fields Penetrating Narrow Slots and Lapped Joints in Thick Conducting Screens," IEEE Trans. Antennas and Prop., Vol. 36, No. 2, pp. 247-257, Feb. 1988.

[8]   R. Luebber, C. Penney, "Scattering From Apertures in Infinite Ground Planes Using FDTD," IEEE Trans. Antennas and Prop., Vol. 42, No. 5, pp. 731-736, May 1994.

[9]   A. Taflove, M. E. Brodwin, "Numerical Solution of Steady-State Electromagnetic Scattering Problems Using the Time-Dependent Maxwell's Equations", IEEE Trans. Microwaves and Theory and Tech., Vol. MTT-23, No. 8, pp. 623-630, Aug. 1975.

[10] A. Taflove, "Application of the Finite-Difference Time-Domain Method to Sinusoidal Steady-State Electromagnetic-Penetration Problems," IEEE Trans. Electromag. Comp., Vol. EMC-22, No. 3, pp. 191-202, Aug. 1980.

[11] A. M. Tran, B. Houshman, T. Itoh, "Analysis of Electromagnetic Coupling Through a Thick Aperture in Multilayer Planar Circuit Using the Extended Spectral Domain Approach and Finite Difference Time-Domain Method," IEEE Trans. Antennas and Prop., Vol. 43, No. 9, pp. 921-926, Sept. 1995.

[12] J. H. Oates and R. T. Shin, "Small Aperture Modeling for EMI applications using the Finite-Difference Time-Domain Technique," Journal of Electromag. Waves and Apps., Vol. 9, No. 1, pp. 37-69, 1995.

[13] C. M. Butler, Y. Rahmat-Samii, R. Mittra, "Electromagnetic Penetration Through Apertures in Conducting Surfaces," IEEE Trans. Antennas and Prop., Vol. AP-26, No. 1, pp. 82-93, Jan. 1978.

[14] W. H. Eggimann, "Higher-Order Evaluation of Electromagnetic Diffraction by Circular Disks," IRE Trans. Microwave Theory and Tech., Sept. 1961, pp. 408-418.

[15] C. M. Butler, "A Formulation of the Finite-Length Narrow Slot or Strip Equation," IEEE Trans. Antennas and Prop., Vol. AP-30, No. 6, pp. 1254-1257, Nov. 1982.

[16] C. M. Butler, K. R. Umashankar, "Electromagnetic Penetration through an Aperture in an Infinite, Planar Screen Separating Two Half Spaces of Different Electromagnetic Properties," Radio Science, Vol. 11, No. 7, pp. 611-619, July 1976.

[17] Lord Rayleigh, "On the Incidence of Aerial and Electric Waves upon Small Obstacles in the form of Ellipsoids or Elliptic Cylinders, and on the Passage of Electric Waves through a circular Aperture in a Conducting Screen," Phil. Mag., Vol 44, pp. 28-52, 1897.

[18] Y. Rahmat-Samii, R. Mittra, "Electromagnetic Coupling Through Small Apertures in a Conducting Screen," IEEE Trans. on Antennas and Prop., Vol. AP-25, No. 2, pp. 180-187, Mar. 1977.

[19] R. B. Kieburtz, A. Ishimaru, "Aperture Fields of an Array of Rectangular Apertures," IRE Trans. on Antennas and Prop., Nov. 1962, pp. 663-671.

[20] L. K. Warne, K. C. Chen, "Slot Apertures Having Depth and Losses Described By Local Transmission Line Theory," IEEE Trans. on Elect. Compat., Vol. 32, No. 3, pp. 185-196, Aug. 1990.

[21] K. Ma, J. L. Drewniak, "A Comparison of FDTD Algorithms for Subcellular Modeling of Slots in Shielding Enclosures," IEEE International EMC Symposium, pp. 157-162, Aug. 1995.

[22] L. K. Warne, K. C. Chen, "A Simple Transmission Line Model for Narrow Slot Apertures Having Depth and Losses," IEEE Trans. on Elect. Compat., Vol. 34, No. 3, pp. 173-182, Aug. 1992.

[23] A. J. Sangster, H. Wang, "A Generalized Analysis for a Class of Rectangular Waveguide Coupler Employing Narrow Wall Slots," IEEE Trans. on Microwave Theory and Tech., Vol. 44, No. 2, pp. 283-290, Feb. 1996.

[24] K. S. Yee, "Numerical Solution of Initial Boundary Value Problems Involving Maxwell's Equations in Isotropic Media," IEEE Trans. Antennas and Prop., Vol. AP-14, No. 3, pp. 302-307, May 1966.

[25] G. Mur, "Absorbing Boundary Conditions for the Finite-Difference Approximation of the Time-Domain Electromagnetic-Field Equations," IEEE Trans. Electromag. Compat., Vol. EMC-23, No. 4, pp. 377-382, Nov. 1981.

[26] K. S. Kunz and R. Luebbers, *The Finite Difference Time Domain Method for Electromagnetics, Boca Raton*; CRC Press, 1993.

[27] Z. P. Liao, H. L. Wong, Y. Baipo, "A Transmitting Boundary for Transient Wave Analyses," Scientia Sinica (Series A), Vol. 27, No. 10, pp. 1063-1076, Oct. 1984.

[28] W. C. Chew, *Waves and Fields in Inhomogeneous Media*, New York, Van Nostrand Reinhold, 1990.

[29] M. Moghaddam, W. C. Chew, "Stabilizing Liao's Absorbing Boundary Conditions Using Single-Precision Arithmetic," Proc. IEEE Antennas and Prop. Soc. Symposium, pp. 430-433, June 1991.

[30] O. M. Ramahi, "Complementary Operators: A Method to Annihilate Artificial Reflections Arising from the Truncation of the Computational Domain in the Solution of Partial Differential Equations," IEEE Trans. on Antennas and Prop., Vol. 43, No. 7, July 1995.

[31] J. L. Young, Frank P. Brueckner, "A Time Domain Numerical Model of a Warm Plasma," Radio Science, Vol. 29, No. 2, pp. 451-463, Mar.-Apr. 1994.

[32] C. J. Railton, E. M. Daniel, "A Comparison of the Properties of Radiating Boundary Conditions in the FDTD Method for Finite Discretisation and Non-Planar Waves," IEEE Trans. on Antennas and Prop., Vol. 42, No. 2, pp. 276-281, Feb. 1994.

[33] J. A. Kong, *Electromagnetic Wave Theory*, 2nd Edition, New York, John Wiley & Sons, 1990.